Top Organomet Chem (2017) 60: 71–112
DOI: 10.1007/3418_2016_12

Published online: 16 March 2017

Functionalization of N_2 by Mid to Late Transition Metals via N–N Bond Cleavage

Isabel Klopsch, Ekaterina Yu Yuzik-Klimova, and Sven Schneider

Abstract This review focuses on the recent efforts to functionalize dinitrogen via complete cleavage of the N≡N bond with particular emphasis on mid to late transition metal complexes. The relationships of electronic and structural parameters for the most common N_2-bonding modes (end-on and side-on bridging) with N_2-splitting reactivity are discussed. This analysis points towards electronic configurations with π^{10} (end-on) and $\pi^8\delta^2$ (side-on) electrons within the M_2N_2-cores for full N–N bond cleavage into terminal and bridging nitride complexes, respectively. The full body of work on N_2-splitting with group 6–8 metals is comprehensively presented. Ligand electronic and steric effects are discussed in detail for privileged platforms, such as low coordinate, electron rich complexes with π-donating ligands. Finally, several strategies for functionalization of the nitrides resulting from N_2-splitting are presented that lead to N–C bond formation. The developed pseudo-catalytic cycles reported so far that combine N_2-cleavage, nitride functionalization, and N-transfer provide guidelines for rational catalyst design.

Keywords Bonding • Dinitrogen splitting • Nitrogen fixation • Transition metal nitrides

Contents

I. Klopsch, E.Y. Yuzik-Klimova, and S. Schneider (✉)
Institute for Inorganic Chemistry, University of Goettingen, Tammannstrasse 4, 37077 Goettingen, Germany
e-mail: sven.schneider@chemie.uni-goettingen.de

1 Nitrogenase, Haber-Bosch, and Catalytic N_2 Fixation

Nitrogen is, next to oxygen, hydrogen, and carbon, one of the main elements found in organic compounds, but atmospheric N_2, which constitutes about 78 vol% of air and more than 99% of global nitrogen, is chemically highly inert. Hence, its conversion into the more reactive nitrogen source ammonia by biological [1, 2] "nitrogen fixation" was crucial for the development of life. Furthermore, our modern societies strongly rely on the industrial Haber-Bosch process [3, 4] for the production of fertilizers and as feedstock for the chemical synthesis of organic nitrogen compounds, the latter consuming approx. 20% of industrially produced NH_3 [5]. Fundamentally different mechanisms were proposed for the conversion of N_2 via these two processes. Nitrogen fixation by the enzyme [Fe,Mo]-nitrogenase proceeds through a series of alternating nitrogen reduction and protonation steps with gradual N–N bond order reduction. In contrast, heterogeneously catalyzed ammonia synthesis proceeds via initial, turn-over limiting dissociative chemisorption of N_2 on the catalyst surface and subsequent stepwise N–H bond formation. These pathways provide the basis for the development of synthetic catalysts that enable the transformation of N_2 at ambient conditions, which is a longstanding goal. To date, a small number of well-defined, biomimetic homogeneous catalysts were reported [6–8]. Alternative electrochemical and photochemical approaches are currently intensively studied, but still suffer from comparatively low selectivities (H_2 evolution) and energy efficiency [9, 10]. Full N_2-splitting into well-defined molecular nitrides was also reported on several instances, but homogeneous catalysts that operate via initial N_2-cleavage remain elusive. However, this approach might offer alternatives to nitrogen fixation beyond NH_3. Molecular nitride chemistry is well developed and several methods for C–N bond formation starting from nitrides are known [11]. Hence, catalysts that directly transform dinitrogen into nitrogen compounds, such as amines, nitriles, or isocyanates, via N_2-splitting and nitride transfer cycles are attractive goals and recent examples that demonstrated stoichiometric routes fuel this idea [5, 12]. In this context, the current review focuses on well-defined molecular systems that enable the functionalization of N_2 via initial full cleavage of the N–N bond with the aim at developing some guidelines that ultimately lead to the design of catalysts for the synthesis of value added nitrogen compounds directly from N_2.

2 Bonding in N_2-Bridged Complexes

2.1 General Considerations

The high bond dissociation (941 kJ mol $^{-1}$) and ionization energies (15.6 eV), low proton (5.1 eV) and electron affinities (−1.9 eV), and the lack of a dipole moment all account for the high thermodynamic and kinetic stability of dinitrogen [13–15]. Cleavage of the first N–N bond defines a major challenge and requires about half of the total triple bond energy (410 kJ mol $^{-1}$). In comparison, acetylene features an even stronger triple bond (962 kJ mol $^{-1}$) but the π-bonds are much weaker (222 kJ mol $^{-1}$), which provides a rationale for the higher reactivity compared with N_2 [16]. A wide range of charge transfer to coordinated N_2-ligands is well documented, reaching from barely activated, neutral N_2 to highly reduced hydrazide $[N_2]^{4-}$ (Table 1). This degree of activation is expressed within spectroscopic (N–N stretching vibration) and structural parameters (N–N bond distance) [17, 18], which are inversely proportional according to Badger's rule [19]. While reduction to diazenide (N_2^{2-}) and hydrazide (N_2^{4-}) ligands are more commonly observed only a few examples for complexes with $[N_2]^{3-}$ radical anion ligands were reported [20]. The monoanionic N_2^- radical was only detected in solid matrix upon photodecomposition of metal azide single crystals and adsorbed on MO (M = Mg, Ca) surfaces at low temperatures [21–24]. According to computations, the unknown free radical species HN_2 is endothermic with respect to decay into N_2 and H by $\Delta E = 9$ kcal/mol and has a lifetime of only around 10^{-10} s at room temperature [25]. Hence, the unfavorable one-electron reduction of N_2 emphasizes the use of multi-electron redox catalysts for nitrogen fixation. The current model for nitrogenase also implies initial two-electron N_2-reduction. These electrons are stored within two Fe–H bonds and charge transfer is triggered by H_2 reductive elimination from the active site [2]. Besides vibrational and structural data, the spin state can also provide information on the redox state of coordinated N_2-ligands due to magnetic coupling of the metal ion with radical ligands, such as N_2^{2-} (S = 1). Alternatively, a covalent picture can be very useful to rationalize bonding with metal ions that have efficient orbital overlap with N_2-ligands (see below).

Four coordination modes of N_2 to metal ions are most frequently found (Fig. 1), i.e., mononuclear end-on (1), dinuclear end-on (2), dinuclear side-on (3), and

Table 1 Bond distances and stretching frequencies for free and coordinated nitrogen species

Free N_2 [26]		1.10 Å	2,331 cm^{-1}
N≡N	S = 0	≈1.10–1.20 Å	≈1,700–2,331 cm^{-1}
$[N{\equiv}N]^-$	S = ½	n.a.	n.a.
Free H_2N_2 [27, 28]		1.25 Å	1,583/1,529 cm^{-1}
$[N{=}N]^{2-}$	S = 1	≈1.20–1.35 Å	≈1,200–1,700 cm^{-1}
$[N{=}N]^{3-}$ [20]	S = ½	1.40 Å	989–1,040 cm^{-1}
Free H_4N_2 [29]		1.45 Å	885 cm^{-1}
$[N{-}N]^{4-}$	S = 0	≈1.40–1.60 Å	≈700–1,100 cm^{-1}

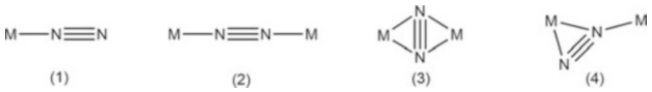

Fig. 1 Most common bonding motifs in N_2 complexes

dinuclear side-on-end-on (4), with (1) being predominant. More than one metal ion will be required for full 6-electron reduction to nitrides. Therefore, only multinuclear activation is discussed in this review. These coordination modes generally show different degrees of N_2-activation, which can be attributed to metal-N_2 bonding and will therefore be discussed in the next two sections for the more common coordination modes (2) and (3). As an important difference, the terminal binding mode (1) and particularly the side-on modes (3) and (4) generally exhibit enhanced reactivity, e.g., with respect to N–H, N–C, or N–Si bond formation. In contrast, such N_2 functionalization reactions were not observed directly for the end-on bridging mode (2). However, (2) proved to be important en route to full N_2-splitting into nitrides, which will be discussed below and in Sect. 3.

2.2 *End-On Bridging N_2*

The end-on bridging mode, M-(μ-η^1-η^1-N_2)-M, is most frequently observed for dinuclear complexes. N_2 activation upon η^1-coordination to the first metal ion increases the electron density on the ligand thus increasing its basicity for binding of the second metal. Charge delocalization over the whole M–N–N–M unit in the dinuclear complex further stabilizes the dinuclear binding motif [30]. End-on bridging N_2-complexes, which are best described by diazenide N_2^{2-} (M–N=N–M) and hydrazide N_2^{4-} (M=N–N=M) resonance structures, are well documented, while radical N_2-ligands (N_2^- or N_2^{3-}) were not reported in this bonding mode [31]. The charge transfer to the N_2-ligand can be rationalized based on orbital interactions as first considered by *Gray* and *Chatt* [32, 33]. N_2 activation is a consequence of back donation from the metal to the N–N π*-antibonding orbitals. In threefold symmetry, two metal d-orbitals (d_{xz}, d_{yz}) are available from each metal ion for π-bonding [46]. Linear combination with the nitrogen π and π* orbitals gives rise to four sets of degenerate π-orbitals ($1e_u$, $1e_g$, $2e_u$, $2e_g$; Scheme 1). It was pointed out in early theoretical work from *Fenske-Hall* computations that mixing of the N–N π-bonding orbitals with metal d-orbitals is weak, i.e., that occupation of the e_u-levels contributes to M–N bonding and N_2 activation to a minor extend [34]. However, the effect of occupation of the $2e_u$ level on N_2 activation was demonstrated by *Cummins* and coworkers within the redox series $[\{(Ar^tBuN)_3Mo\}_2(\mu\text{-}\eta^1\text{:}\eta^1\text{-}N_2)]^{n+}$ (n = 0–2; Fig. 2; see below for discussion). Besides the M–N–N–M π-manifold, the frontier orbitals are complemented by M–N bonding MOs (a_u/a_{2u}) that result from mixing of metal d_{z2}-orbitals with the N–N σ-antibonding orbital [37, 101]. This MO is strongly N–N antibonding in

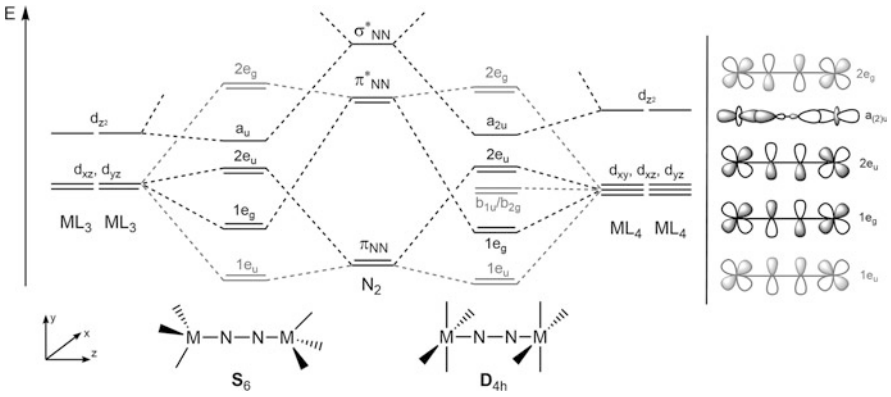

Scheme 1 Qualitative orbital interaction diagram for end-on N_2 bridged dinuclear complexes in threefold and fourfold geometry (*left*) and symmetry of the M–N–N–M σ- and π-type MOs (*right*) as an extension of *Fryzuk's* scheme [46]. MOs less relevant for N_2-activation and splitting drawn in *grey*

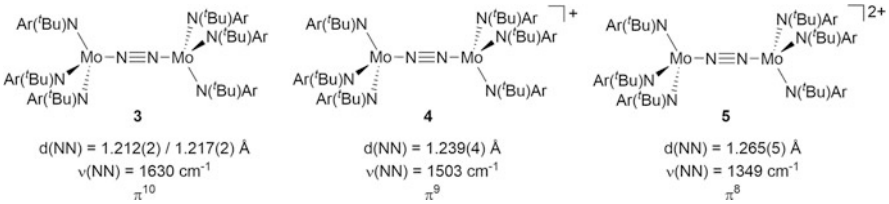

Fig. 2 Bond distances, stretching frequencies, and number of electrons in the MNNM π-system for $\{Mo[N(tBu)(Ar)]_3\}_2(\mu\text{-}\eta^1\text{-}\eta^1\text{-}N_2)^{n+}$ ($n = 0$–2) [36, 37]

nature. Hence, its occupation strongly weakens the N_2 bond. Furthermore, it drops in energy upon splitting the N_2-complex into terminal nitrides (see Scheme 7). In addition to these σ– and π–M_2N_2 interactions, in fourfold symmetry (octahedral or square pyramidal geometry) two metal-based non-bonding MOs with δ/δ*-character are derived from d_{xy}. In threefold symmetry these MOs should be much higher in energy due to interaction with the auxiliary ligands.

Based on this simple qualitative MO scheme, the degree of N_2-activation can be correlated to π-orbital occupancy within closely related systems upon filling the MOs with the four electrons from N_2 π-bonding and the valence electrons contributed from the two ML_n fragments. Occupation of the e_g levels weakens the N–N bond in contrast to the MOs with e_u symmetry. Hence, it is evident that a π^8 valence electron configuration should result in maximal N_2 bond weakening. For example, the N_2-bridged dirtuthenium complex $[(NH_3)_5RuN_2Ru(NH_3)_5]^{4+}$ (**1**) exhibits a π^{12} configuration $((1e_u)^4(1e_g)^4(b_{1u})^2(b_{2u})^2(2e_u)^4(2e_g)^0)$ with a very small degree of N_2 bond weakening ($d_{NN} = 1.12$ Å, $\nu_{NN} = 2{,}100\ cm^{-1}$) [32]. In contrast, the bimetallic complex $[(PMe_2Ph)_4ClReN_2MoCl_4(OMe)]$ (**2**) with π^8 configuration $((1e_u)^4(1e_g)^4$

$(b_{1u})^2(b_{2u})^1(2e_u)^0(2e_g)^0$) displays much stronger N_2-activation (d_{NN} = 1.21 Å, ν_{NN} = 1,660 cm^{-1}) [35].

This dependence of the degree of activation on valence electron configuration is nicely reflected within the redox series $[\{(ArtBuN)_3Mo\}_2(\mu\text{-}\eta^1\text{:}\eta^1\text{-}N_2)]^{n+}$ (n = 0 (**3**), 1 (**4**), 2 (**5**); Ar = 3,5-$C_6H_3Me_2$; Fig. 2) reported by *Cummins* and coworkers [36, 37]. According to this model, these compounds adopt $(1e_u)^4(1e_g)^4(2e_u)^{(2\text{-}n)}(2e_g)^0$ configurations, i.e., 10 (n = 0, **3**), 9 (n = 1, **4**), and 8 (n = 2, **5**) electrons in Mo–N–N–Mo π-type orbitals, respectively. The electronic triplet (**3**), doublet (**4**), and singlet (**5**) ground states and the increasing activation upon oxidation of the parent π^{10} system **3** (Fig. 2) are in agreement with the bonding model. Interestingly, while **4** and **5** are thermally stable, only the supposedly least activated N_2-complex **3** splits into the terminal nitrides [NMo(N*t*BuAr)$_3$] [38]. Splitting of the π^{10}-dimer **3** produces two closed shell, pseudo-tetrahedral molybdenum(VI) nitrides. As the N–N σ-antibonding a_u-orbital drops in energy upon splitting, two electrons are transferred from the π- to the σ-manifold (Scheme 7). In comparison, the oxidized dimers **4** and **5** are short by one and two electrons, respectively, to form nitrides where all M–N σ- and π-bonding orbitals are fully occupied. These simple considerations emphasize the preference for a π^{10}-configuration in splitting of linearly N_2-bridged dinuclear complexes into terminal nitrides. The same arguments were applied to analogous systems, which are discussed in more detail in Sect. 3.

The subtle influence of different metals within strongly related coordination spheres on N_2-activation was systematically examined by *Sita* and coworkers. They reported a series of group 4–6 η^5-cyclopentadienyl/η^2-amidinate complexes (am = N(*i*Pr)C(Me)N(*i*Pr); M = Ti (**6**), Zr (**7**), Hf (**8**), V (**9**), Nb (**10**), Ta (**11**), Mo (**12**), W (**13**); Fig. 3 and Table 2) [39–41]. Except for Zr and Hf, isostructural end-on bridging N_2-coordination was found. The diamagnetic Ti-complex **6** was described as two Ti^{III} d^1-ions spin-coupled with an N_2^{2-} bridge. The high fourth ionization potential of Ti prevents further reduction of N_2 [42]. Slightly less activation was observed for the analogous vanadium complex **9**, leading to the description as two antiferromagnetically coupled V^{II}-ions bridged by N_2, which qualitatively reflects the decreased reduction potential compared with titanium. The higher degree of activation for the niobium and tantalum dimers **10** and **11** also reflects the trends in reduction potential upon moving down group 5. These compounds were described as containing Ta^{IV} and Nb^{IV}, respectively, which are bridged by $[N_2]^{4-}$ ligands. For **11**, preliminary magnetic data supported a singlet ground state and thermally populated triplet state with antiferromagnetic exchange above 2K. **11** also splits the strongly reduced N_2-ligand to form the tantalum(V)

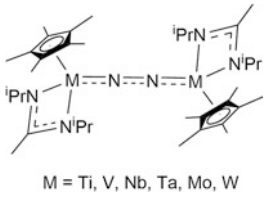

Fig. 3 *Sita*'s isostructural $(Cp^*amM)_2(\mu\text{-}N_2)$ complexes

Table 2 N–N bond distances in $(Cp^*amM)_2(\mu\text{-}N_2)$ complexes

Metal	Coordination mode	d(NN) [Å]	Reference
Ti (**6**)	$(\mu\text{-}\eta^1\text{-}\eta^1\text{-}N_2)$	1.270(2)	[40]
Zr[a] (**7**)	$(\mu\text{-}\eta^2\text{-}\eta^2\text{-}N_2)$	1.518(2)	[43]
Hf (**8**)	$(\mu\text{-}\eta^2\text{-}\eta^2\text{-}N_2)$	1.611(4)	[43]
V (**9**)	$(\mu\text{-}\eta^1\text{-}\eta^1\text{-}N_2)$	1.225(2)	[41]
Nb[b] (**10**)	$(\mu\text{-}\eta^1\text{-}\eta^1\text{-}N_2)$	1.300(3)	[41]
Ta (**11**)	$(\mu\text{-}\eta^1\text{-}\eta^1\text{-}N_2)$	1.313(4)	[39]
Mo (**12**)	$(\mu\text{-}\eta^1\text{-}\eta^1\text{-}N_2)$	1.267(2)	[40]
W (**13**)	$(\mu\text{-}\eta^1\text{-}\eta^1\text{-}N_2)$	1.277(8)	[40]

[a]Exchange of methyl group in amidinate against NMe_2
[b]Exchange of methyl group in amidinate against phenyl

nitride bridged complex $[\{Cp^*(am)Ta\}_2(\mu\text{-}N)_2]$ above 0°C. In turn, the diamagnetic group 6 analogues **12** and **13** are again in agreement with decreasing reduction potential and show weaker activation of the N_2 bridge compared to Nb and Ta. While **12** and **13** are thermally stable, N_2-splitting was realized photochemically (c.f. Sect. 3).

Strong ligand influences on N_2-activation are also well documented. An instructive example was provided by the group of *Chirik*, who reported the isolation of the extensive terpyridine dimolybdenum dinitrogen series $[\{(^{Ph}Tpy)(PPh_2Me)_2Mo\}_2(\mu\text{-}\eta^1\text{:}\eta^1\text{-}N_2)][BAr^F{}_4]_n$ ($n = 0$ (**14**), 1 (**15**), 2 (**16**), 3 (**17**), 4 (**18**); Scheme 2) [44]. Spectroscopic data of the dicationic complex **16** indicates an N_2^{2-} bridge. DFT computations support a $\pi^{10}(\delta^4)$ configuration, yet with a singlet ground state as the degeneracy of the frontier π^*-MOs is strongly lifted due to electronic coupling with the Tpy ligand. Single and double oxidation leads to stronger N_2-activation as the electrons are removed from the N–N bonding π^*-orbital. Intriguingly, reduction also results in N–N bond weakening since the SOMO of **15** is Tpy-ligand centered, which was also found for the second reduction. The use of redox active ligands for electron storage provides an attractive approach for multi-electron redox reactions like nitrogen fixation.

2.3 *Side-On Bridging N_2*

The side-on N_2-bridging coordination mode is less common in dinuclear complexes than end-on coordination [17, 45, 46]. First evidence was provided by the linkage isomerization of the isotopomers of $[(NH_3)_5Ru(^{14/15}N_2)]^{2+}$ which is too fast to proceed via N_2 dissociation, suggesting intermediate side-on coordination [47]. The first structurally characterized side-on N_2 complex, a polynuclear nickel-lithium compound, was reported in 1973 [48, 49]. By now, several other examples were reported, mostly with early transition metals and f-block elements, exhibiting varying degrees of activation, as exemplified by *Evans'* $[(Cp^*_2Sm)_2(\mu\text{-}\eta^2\text{:}\eta^2\text{-}N_2)]$ (**19**, $d_{NN} = 1.088(12)$ Å) vs. *Fryzuk's* $[\{(PNP)ZrCl\}_2(\mu\text{-}\eta^2\text{:}\eta^2\text{-}N_2)]$ (**20**,

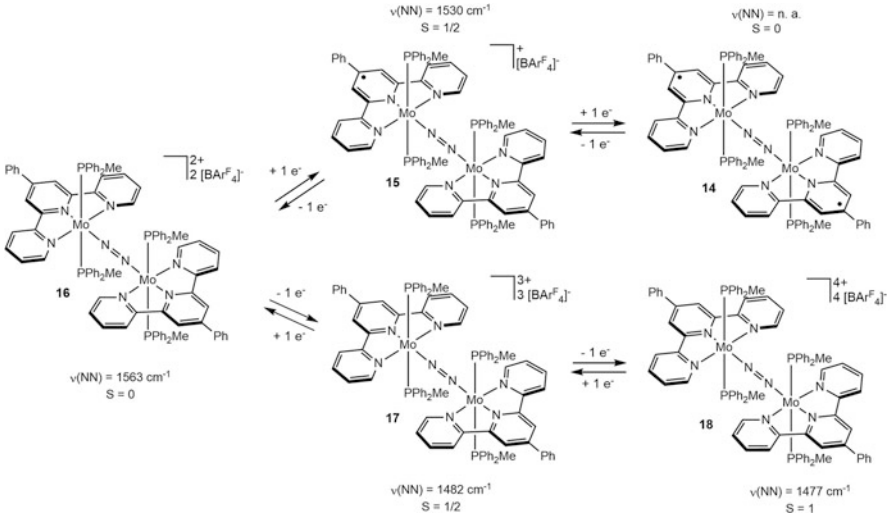

Scheme 2 $[\{(^{Ph}Tpy)(PPh_2Me)_2Mo\}_2(\mu\text{-}\eta^1\text{-}\eta^1\text{-}N_2)][BAr^F{}_4]_n$ (n = 0–4) redox series reported by *Chirik* and coworkers [44]

[PNP] = $(i Pr_2PCH_2SiMe_2)_2$ N) (d_{NN} = 1.548(7) Å) [50, 51]. Bonding of the two metal centers with side-on bound N_2 is more complex compared with the end-on isomer, as considerable distortion from planarity of the M_2N_2 core is often observed. A simplified model for two side-on N_2-bridged square-pyramidal ML_4 fragments is shown in Scheme 3, based on considerations first described by *Fryzuk* and coworkers [46]. Metal N_2 bonding should be dominated by back donation from suitable d-orbitals into the N_2 π*-orbitals. In contrast to end-on coordination, only one π-interaction results from out of phase combination of the two d_{xz} orbitals and the horizontal N_2 π*-level. In addition, an interaction with δ-symmetry is constructed by the in-phase d_{xy} combination with the vertical N_2 π*-orbital. Both MOs are N–N antibonding in character. However, weaker orbital overlap for the δ- with respect to π-interactions suggests an energetic preference for end-on N_2-coordination. In fact, isolable mononuclear complexes with side-on terminal η^1-η^1-N_2-coordination remain unknown [52].

One reason for the occurrence of side-on bridging N_2-ligands can be the absence of an accessible d-orbital that is suitable to form the second π-bond. Semi-empirical computations for the model complex $[\{Zr(Cl)N(SiH_2CH_2PH_2)_2\}_2(\mu\text{-}\eta^2\text{:}\eta^2\text{-}N_2)]$ confirmed this picture revealing that one of the d-orbitals required for π-bonding is raised in energy due to π-donation by the amide and chloride ligands [46]. In fact, ligand exchange of chloride vs. cyclopentadienide (Cp) results in N_2 linkage isomerization and isolation of the end-on bridged complex $[\{(PNP)ZrCp\}_2(\mu\text{-}\eta^1\text{:}\eta^1\text{-}N_2)]$ (**21**, Scheme 4) [46]. Hence, exchange of chloride by Cp stabilizes the end-on coordination by reducing the Cl^-/N_2 π-MO competition and destabilizes the side-on coordination as the Cp ligand overlaps with a d-orbital that would be required for

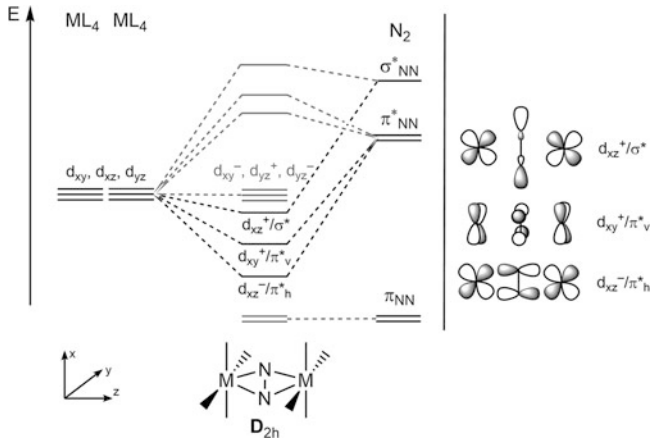

Scheme 3 Qualitative orbital interaction diagram for side-on N_2 bridged dinuclear complexes (*left*) and symmetry of the relevant MOs (*right*) as an extension of *Fryzuk's* scheme [46]. MOs less relevant for N_2-activation and splitting drawn in *grey*

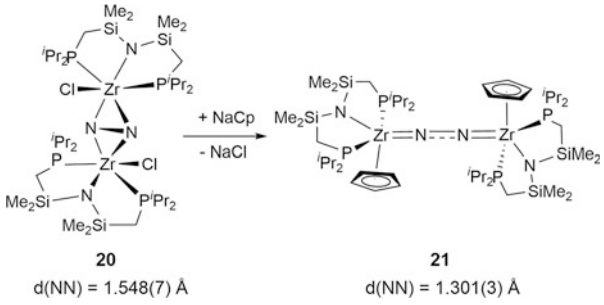

Scheme 4 Transformation of side-on to end-on N_2 configuration by ligand exchange [46]

δ-bonding with a side-on N_2 complex. The remaining N_{amide}–Zr–N_2 π-interaction is expressed in an unusually long Zr–N_{amide} bond of **21** (2.306(3)/2.303(3) Å) [53, 54]. Bonding analysis of the zirconium system on a higher computational level (DFT) by *Tuczek* and coworkers qualitatively confirmed the earlier picture and showed that distortion of the M_2N_2 core from planarity to a butterfly structure aids at charge delocalization of the N_2-ligand [55]. Furthermore, the LUMO was described as a non-bonding, metal-based MO from out of phase combination of two d_{xy} orbitals (d_{xy}^-). Slightly higher, an MO was found from combination of metal d-orbitals with the N_2 σ*-orbital (drawn below d_{xy}^- in simplified Scheme 3). Occupation of this MO should strongly weaken the N–N bond. However, the Zr_2N_2 core does not contain enough electrons for full N_2 cleavage. In contrast, model computations for [{$SiMe_3N(CH_2CH_2NSiMe_3)_2V$}$_2$(μ-$\eta^2$:$\eta^2$-$N_2$)], which in fact splits the N_2-ligand into the dinitride bridged divanadium(V) isomer [56], indicate the population of such an MO with N_2 σ*-character [57, 58]. Together

with the filled N_2 π-orbitals, this picture emphasizes an overall $\pi^8\delta^2$ valence electron configuration to be favorable for N_2-splitting for the side-on coordination. Importantly, comparison of the two simplified MO-schemes for end-on (D_{4h}) and side-on (D_{2h}) coordination suggests that a lower valence electron count of the ML_4 fragments is required for splitting from the side-on linkage isomer. This is in fact corroborated by computational DFT analysis of the conversion of [{Cp*(am)Ta}$_2$(μ-N_2)] into [{Cp*(am)Ta}$_2$(μ-N)$_2$] [41, 59]. The proposed mechanism proceeds via initial isomerization of the triplet end-on (π^8) to the singlet side-on ($\pi^8\delta^2$) form prior to N_2-splitting, in full agreement with this very simple model.

The electronic structures of [{R_2M}$_2$(μ-η^2:η^2-N_2)] (M = group 4–9, R = amide, cyclopentadienide) complexes with planar M_2N_2-cores were examined computationally by *Stranger* and coworkers [60]. An increase in activation was found upon descending a group, presumably due to more diffuse d-orbitals resulting in better overlap. Furthermore, the conformation of M(NH_2)$_2$ fragments with respect to the M_2N_2-core was predicted to have a strong impact on N_2 activation and cleavage. In general, perpendicular arrangement leads to stronger activation due to better electron delocalization into the MNNM moiety. Moving along the transition series eventually results in N_2-splitting as predicted by the simple model in Scheme 3. Additional metal–metal interactions stabilize the nitride bridged products.

Besides these electronic considerations, sterics also play an important role, as the two metal moieties are closer in the side-on bonding mode. This was demonstrated for a series of zirconocenes [61, 62]. In contrast to *Bercaw's* classic decamethylzirconocene dimer [{Cp*$_2$Zr(η^1-N_2)}$_2$(μ-η^1-η^1-N_2)] (**22**; Cp* = C_5Me_5) and analogous [{Cp*Cp′Zr(η^1-N_2)}$_2$(μ-η^1:η^1-N_2)] (**23**; Cp′ = C_5Me_4H), removal of a second methyl group results in the side-on bridged octametylzirconocene dimer [(Cp′$_2$Zr)$_2$(μ-η^2:η^2-N_2)] (**24**) with side-on bridging N_2 (Fig. 4) [63–65]. DFT calculations predict the relative stability of side-on N_2 bridged isomers to increase down group 4 in the periodic table [42]. This trend is confirmed experimentally for the series [(Cp*amM)$_2$(μ-N_2)] (M = Ti, Zr, Hf), which exhibits end-on for Ti (**6**) and side-on configuration for the Zr (**7**) and Hf (**8**) complexes (Table 2) [40]. It is assumed that only the larger Zr and Hf (ionic radii: 1.75 Å) are able to accommodate the more crowded side-on coordination, while the smaller homologue Ti (1.60 Å) and other metals like V (1.53 Å), Nb (1.64 Å), or Mo (1.54 Å) adopt the end-on bonding motif with this ligand set.

An important difference between end-on and side-on bridging coordination is the reactivity. In fact, the only N_2-functionalization reaction that is known for the end-on bridging mode is splitting into nitrides. In contrast, reactions like C–N coupling with CO, which can lead to full scission of the N–N bond, are well

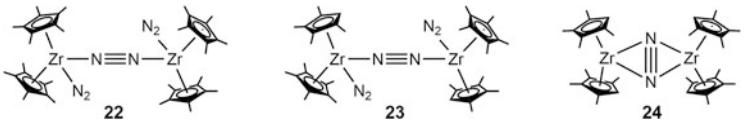

Fig. 4 Steric effect on end-on vs. side-on N_2 binding

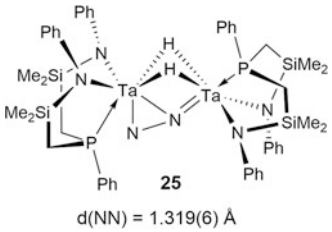

Fig. 5 Side-on end-on N_2 bridged tantalum complex [68]

documented for side-on bonding [63, 66] and computations indicate that side-on binding is a prerequisite for N_2-hydrogenation [67]. Related reactivity was also observed for the rare, side-on/end-on coordination mode, e.g., for [{(NPN)Ta}$_2$(-μ-H)$_2$(μ-η^1:η^2-N_2)] (**25**, NPN = (Ph)P(CH_2SiMe_2NPh)$_2$) (Fig. 5) [68, 69]. This compound is formed upon reaction of dinuclear Ta(IV) hydride complex [{(NPN)Ta}$_2$(μ-H)$_4$] (NPN = PhP(CH_2SiMe_2NPh)$_2$) with N_2 under partial release of H_2. Hence, the reducing equivalents for N_2 reduction are stored in two Ta–H bonds providing an early model for nitrogenase reactivity. The energetic advantage of maintaining the remaining bridging hydrides, which force the two metal centers in **25** in close proximity, is believed to prevail over the energy difference to dinuclear end-on coordination. Subsequent treatment with boranes [70], silanes [71–73], alanes [74], zirconocenes [75], or with 1,2-cumulenes [76] led to full cleavage of the dinitrogen bond.

3 Splitting of N_2 into Nitride Complexes of Group 6 Elements and Beyond

As discussed in Sect. 2, the type of metal, oxidation state, coordination geometry, ligand type, and electronic configuration are essential features that govern the ability of N_2-bridged multinuclear complexes to split into nitrides. In this section, we want to illustrate these principles with a comprehensive overview over N_2-splitting reactions mediated by mid to late transition metal complexes (group 6-8). Other examples from group 4-5 and f-block chemistry are not part of this section, but will be covered by other reviews in this book.

3.1 N_2-Splitting by Homoleptic Group 6 Amide Complexes

Arguably the best examined system regarding both N_2-splitting and transfer of the resulting nitride ligands is *Cummins'* molybdenum triamides, which also marks the first example for N_2-cleavage into well-defined nitrides [36, 38]. [(Ar*t*BuN)$_3$Mo(μ-η^1-η^1-N_2)Mo(N*t*BuAr)$_3$] (**3**, Ar = 3,5-$C_6H_3Me_2$) forms upon reaction of the isolable molybdenum(III) complex [Mo(N*t*BuAr)$_3$] (**26**) at −35°C under N_2

(1 atm) and splits into the molybdenum(VI) nitrides [NMo(N*t*BuAr)$_3$] (**27**) when warmed to room temperature (Scheme 5) in near quantitative yield. N_2-splitting was computed to be exothermic by about 20 kcal/mol [77], but N_2-uptake on this route requires several days. It can be significantly accelerated by addition of reductants, and isolation of terminal dinitrogen complex Na[(N$_2$)Mo(N(*t*Bu)Ar)$_3$] (**28**) allowed for the proposal of a redox-catalytic mechanism (Scheme 6) [78].

The spectroscopic, magnetic, and structural features of intermediate **3** indicate moderate to strong N_2-activation, in agreement with $Mo^{IV}\{N_2^{2-}\}Mo^{IV}$ and the covalent π^{10} bonding model described above [36, 37]. The reaction can also be rationalized by extension of the π-MO scheme in the dimer. Full splitting into nitride complexes requires additional charge transfer to the N_2-ligand, more exactly form the $2e_u$ π-orbitals to the a_u σ*-MO of triplet **3** (Scheme 7), which drops in energy upon N–N bond cleavage and formation of the closed-shell molybdenum (VI) nitride products. Hence, dissociation of the dimer along the N–N bond vector is symmetry forbidden but requires breaking of the high symmetry of **3** (S_6) for σ/π-MO-mixing. Accordingly, *Morokuma* and coworkers computed a zigzag transition state (TS) with approximate N–N single bond character for model complex [(NH$_2$)$_3$MoN$_2$Mo(NH$_2$)$_3$]$_2$ [77]. In the TS the antibonding character of the $3b_u$ is reduced upon M–N–N–M bending and mixing with the $2b_u$ orbital enabling charge

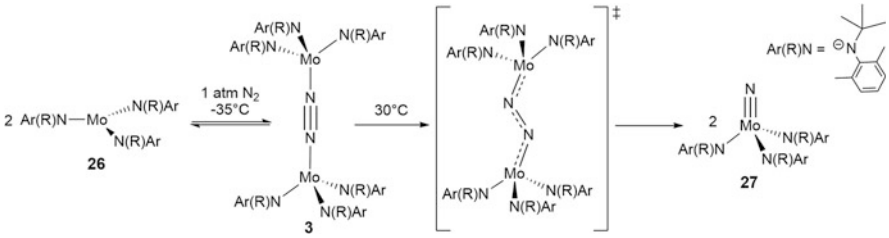

Scheme 5 Cleavage of N_2 in terminal nitrides mediated by a triamido molybdenum(III) complex [38]

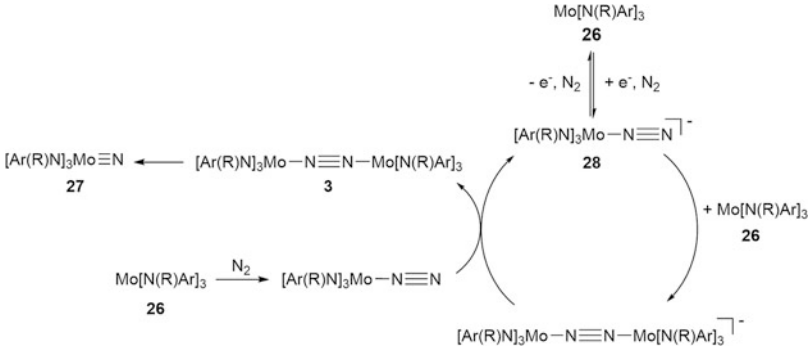

Scheme 6 Redox-catalytic mechanism for N_2-splitting from **26** into **27** [78]

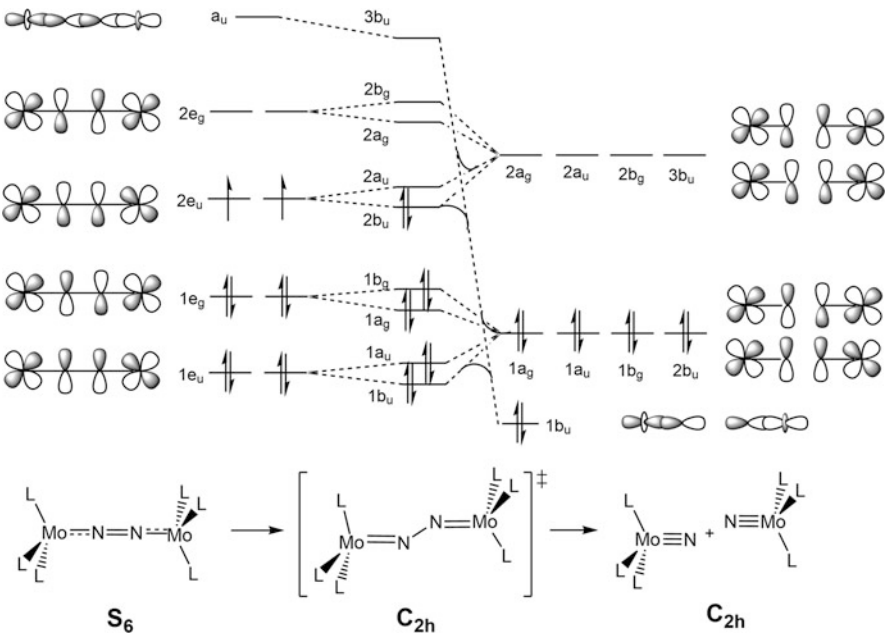

Scheme 7 MO scheme for N_2 cleavage in terminal nitrides out of a Mo(III) dinuclear dimer in S_6 symmetry [36]

transfer to the nitride. This picture also resolves the apparent dichotomy observed for the oxidized compounds $[(Ar\mathit{t}BuN)_3Mo(\mu\text{-}\eta^1\text{-}\eta^1\text{-}N_2)Mo(N\mathit{t}BuAr)_3]^+$ (**4**) and $[(Ar\mathit{t}BuN)_3Mo(\mu\text{-}\eta^1\text{-}\eta^1\text{-}N_2)Mo(N\mathit{t}BuAr)_3]^{2+}$ (**5**). While the π^9 (**4**) and π^8 (**5**) configurations exhibit stronger N_2 activation (see Sect. 2) in the ground state, they are short by one and two electrons, respectively, to split into stable closed-shell nitrido complexes.

An interesting comparison is given with *Schrock*'s related triamidoamine dimer $[\{(R'NCH_2CH_2)_3NMo\}_2(\mu\text{-}\eta^1\text{:}\eta^1\text{-}N_2)]$ (**29**, $R' = \mathit{t}BuMe_2Si$) [36, 79, 80]. Both **3** and **29** exhibit the same formal oxidation and spin states and display similar structural parameters within the central Mo–N–N–Mo moiety. However, *Schrock*'s dimer does not split into the respective nitrides (Scheme 8), which could be prepared on another route. This observation can be attributed to the *trans*-influence of the additional amine donor, which destabilizes σ-bonding with the nitride ligand and the a_u orbital in the dimer. Hence, splitting is both thermodynamically and kinetically more unfavorable and splitting of a simplified model of **29** was calculated to be endothermic [77]. Computational work on truncated models by *Stranger* and coworkers suggests that the conformational rigidity of the triamidoamine vs. the monodentate amido ligands might also contribute to the difference in reactivity [81, 82]. Rotation of an amido ligand by 90° increases charge transfer from the metal to N_2 (Scheme 9). This conformation also stabilizes an electronic singlet with respect to the triplet state, en route to the singlet zigzag transition state. However, in

Scheme 8 Comparison of *Schrock*'s triamidoamine Mo(III) and *Cummins´* triamido Mo(III) N_2 dimers towards N_2 cleavage

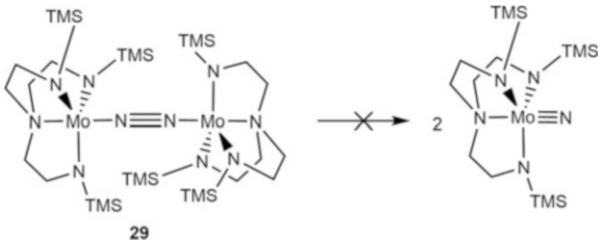

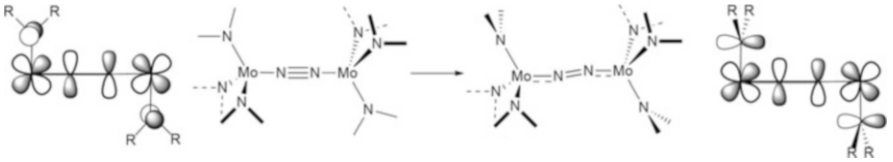

Scheme 9 Rotation of one NR_2 group at each Mo center in $[Mo(NR_2)_3]_2(\mu\text{-}N_2)$

agreement with the experimentally confirmed triplet ground state of **3** [37], computations on full **3** revealed that the bulky *tert*-butylanilide ligands strongly destabilize the singlet and N_2-splitting might in fact not pass through this intermediate [83].

π-Donor ancillary ligands generally lead to stronger N_2 activation and more exothermic splitting [77, 81]. In fact, the triaryl analogue $[(Mes_3Mo)_2(\mu\text{-}\eta^1\text{:}\eta^1\text{-}N_2)]$ (**30**, Mes = 2,4,6-$Me_3C_6H_2$) reported by *Floriani* and coworkers is stable in refluxing benzene [84]. However, irradiation in the UV range (λ = 365.0 nm) produces the nitride bridged dimer $[(Mes_3Mo)_2(\mu\text{-}N)]$ (**31**), which marked the first example of photochemical N_2-splitting. The authors proposed a mechanism (Scheme 10, top) via initial photolysis into monomeric nitrides, which form a transient tetranuclear intermediate with parent **30** and finally the nitride bridged dinuclear product **31** after N_2-loss. *Cummins* proposed an alternative mechanism based on detailed examination of the trianilide platform. Bulk irradiation of **3** with visible light ($\lambda \geq$ 480 nm) at −78°C produces a 1:1 mixture of nitride **27** and parent $[Mo(N\mathit{t}BuAr)_3]$ **26** (Scheme 10, bottom) [37]. Frequency resolved pump-probe spectroscopy revealed that excitation at 2.3 eV creates an excited triplet state, which relaxes through internal conversion (IC) within 300 fs. to a vibrationally excited ground state [85]. Rapid cooling of the hot ground state (sub-ps) explains the modest quantum yield (Φ = 0.05) for the two Mo–N and N–N dissociative reaction channels. Importantly, coupling of IC with structural distortions of the Mo–N–N–Mo core facilitates the entry into the higher barrier N–N cleavage channel through the singlet zigzag transition state and thereby compensates the thermal bias for Mo–N cleavage, which results in the photochemical 1:1 product mixture. Such distortions were predicted computationally for the photochemical states of linearly bridged diiron and -ruthenium μ-N_2 complexes (M = Fe, Ru) by *Reiher* et al. [86].

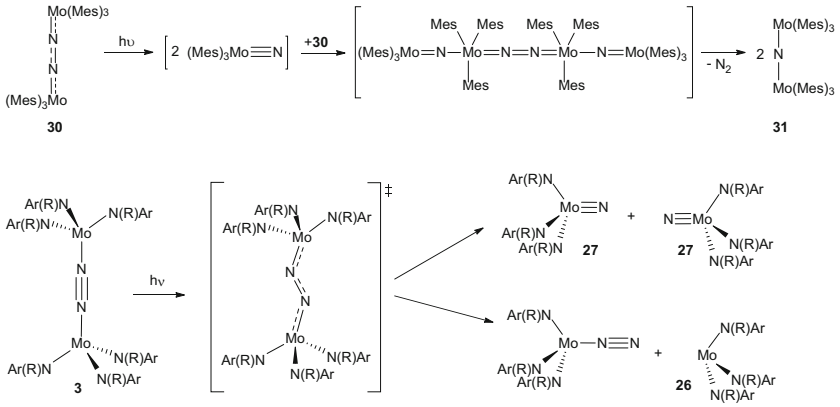

Scheme 10 Proposed photolysis mechanisms for *Floriani*'s dimer **30** (*top*) and *Cummins´* dimer **3** (*bottom*) [37, 84]

The necessity for **3** to distort from linearity for N–N bond cleavage indicates that ligand sterics are crucial not only for the formation of N_2-bridged complexes but also for splitting into nitrides. For example, [Mo(NAdAr)$_3$] (Ad = 1-adamantyl) does not form nitrides under N_2, presumably due to the excessive steric bulk of the amide ligands [78]. However, steric shielding is required to prevent metal–metal bonding and formation, as found for $Mo_2(NR_2)_6$ (NR_2 = NMe_2, NMeEt, NEt_2), which do not react with N_2 (Scheme 11, top) [87]. These considerations were confirmed by DFT computations [88]. For the same reason, use of alkoxide ligands was unsuccessful, although rapid nitride transfer between the alkoxide and amide platforms was demonstrated (Scheme 11, mid) [89–91]. N_2-splitting with a smaller ispropylamide ligand was also reported (Scheme 11, bottom). However, in case of the *iso*-propylanilide metal–metal bond formation is suppressed by reversible methyne C–H cyclometalation [92]. Reaction of [MoH(η^2-Me_2C=NAr)(N*i*PrAr)$_2$] (**32**) with N_2 gives the nitride bridged complex [{(Ar*i*PrN)$_3$Mo}$_2$(μ-N)] (**33**). The proposed mechanism implies a CH reductive elimination preequilibrium, N_2-splitting, and dimerization with the parent triamide. Mixing **32** and [NMo(N*i*PrAr)$_3$] gives the same product.

3.2 N_2-Splitting by Group 6 and 7 Pincer Complexes

Tridentate, monoanionic, meridionally coordinating ("pincer") ligands are extensively used in small molecule activation and homogeneous catalysis [93, 94]. Bulky substituents aid in enforcing rigid square-planar, square-pyramidal, or octahedral coordination geometries and direct the reactivity to predefined sites. Four accounts on N_2 cleavage into nitrides with group 6 and 7 complexes were reported that carry pincer-type or related ligands. *Schrock* pointed out that N_2 activation with

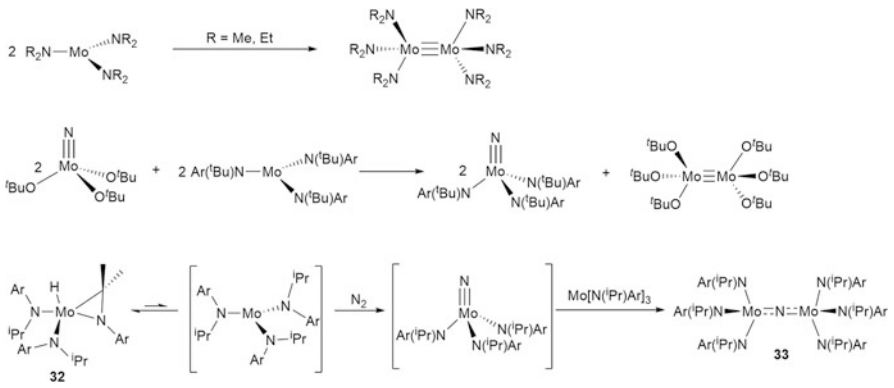

Scheme 11 Dimerization of molybdenum triamides/trialkoxides

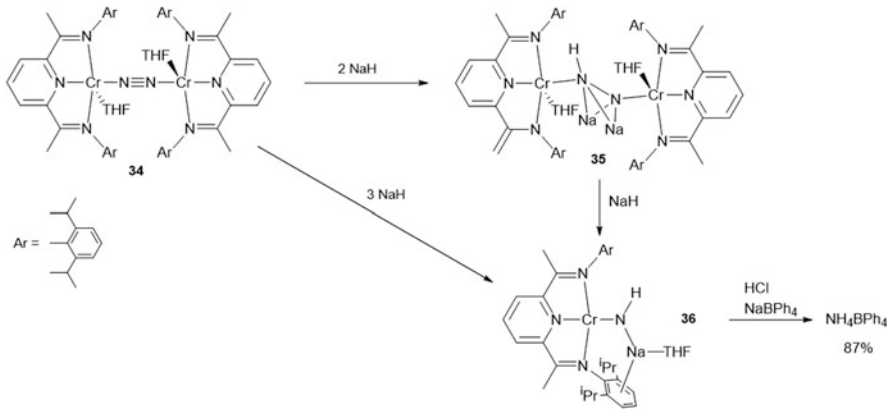

Scheme 12 N_2 cleavage by reduction of a chromium N_2 bridged dimer with NaH [96]

chromium is more difficult compared with molybdenum due to low lying high-spin states and the weak reduction potential of Cr^{III}-compounds [95]. In addition, DFT calculations by *Stranger* predict unfavorable thermochemistry of N_2-splitting for chromium triamides [81]. Regardless, *Budzelaar*, *Gambarotta*, and coworkers reported N_2-cleavage mediated by a well-defined chromium complex [96]. Reduction of N_2 bridged $[\{(NNN)Cr(THF)\}_2(\mu{:}\eta^1\text{-}\eta^1\text{-}N_2)]$ (**34,** NNN=C_5H_3N-2,6-{2,6-(^{i} $Pr_2C_6H_3$)N=$C(CH_3)$}$_2$) with 2 eq. of NaH led to the protonated hydrazide species **35** (Scheme 12). The hydrogen atom of the N_2H ligand was transferred from a methyl group of the diimine ligand. Treatment with an additional equivalent NaH results in full N–N bond scission and formation of imide **36**. Ammonia could be collected in 87% yield after addition of aqueous HCl.

Schrock and coworkers reported full N_2-cleavage into terminal nitrides for the reduction of molybdenum(III) pincer complex [MoI_2(POCOP)] (**37**, POCOP=C_6H_3-

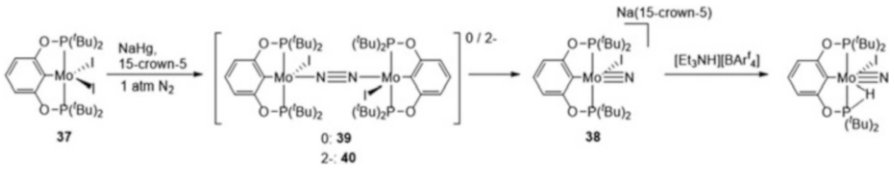

Scheme 13 N_2 cleavage and subsequent protonation of the terminal nitride in *Schrock*'s {(POCOP)Mo} system [97]

2,6-$(OP^tBu_2)_2$) with Na/Hg under N_2 in the presence of crown ether 15-crown-5 (Scheme 13) [97]. The square-pyramidal, diamagnetic nitrido molybdate(IV) [Na(15-crown-5)][Mo(N)I(POCOP)] (**38**) was isolated. The authors proposed a mechanism via an end-on N_2-bridged dinuclear intermediate, which splits into nitrides, in analogy with *Cummins'* molybdenum trianilide system. Two reducing equivalents are overall required per {Mo(POCOP)} moiety which raises the question about the electronic configuration of the state that undergoes N–N bond scission. The authors favored cleavage on the neutral [(POCOP)IMo(N_2)MoI(POCOP)] (**39**) stage into intermediate molybdenum(V) nitrides over splitting of [(POCOP)IMo(N_2)MoI(POCOP)]$^{2-}$ (**40**) into the final molybdenum(IV) product. Within a simplified covalent binding model in idealized fourfold symmetry (Scheme 1), the Mo–N–N–Mo core of neutral dimer **39** exhibits a π^8 electronic configuration (in case of low spin) vs. π^{10} expected for dianionic **40**. Within this simple isolobal analogy the putative dianionic π^{10} dimer **40** with Mo in square-pyramidal geometry resembles *Cummins*' π^{10} trianilide dimer **3** in threefold symmetry more closely. Alternatively, splitting of **39** implies additional charge transfer from the metal to the N_2-ligand when starting from a singlet π^8 ground state, e.g., by crossing to a π^{10} quintet en route to a molybdenum(V) nitride splitting product, which is then further reduced to final **38**. Experimental or computational information about the reaction pathway or the structures and spin-states of intermediates are not yet available. Protonation of the molybdenum(IV) nitrido complex **38** with $[Et_3NH][BAr^F{}_4]$ leads to formation of a hydride species in which the proton bridges the metal ion and a phosphorous ligand. Nitride protonation was not observed and with a mixture of organometallic reductants and acid only around 0.3 equivalents of ammonia were detected.

In analogy to *Schrock's* pincer system, the group of *Mézailles* reported N_2-splitting upon reduction of molybdenum trichloride [$MoCl_3(PPP^{Cy})$] (**41**, PPP^{Cy} = PhP$(CH_2CH_2PCy_2)_2$) with Na/Hg in the presence of NaI under N_2 atmosphere [98]. The terminal nitride [Mo(N)I(PPP^{Cy})] (**42**) was observed in 80% spectroscopic and 60% isolated yield (Scheme 14). The authors also proposed N_2-cleavage of dinuclear intermediate [{(PPP^{Cy})IMo}$_2$(μ:η^1-η^1-N_2)] (**43**) into the nitride **42**. Notably, such an intermediate should have a π^{10} electronic configuration resembling the *Cummins* dimer **3**. Interestingly, the molybdenum(0) complexes [{(PPP^{Cy})$(N_2)_2$Mo}$_2$(μ:η^1-η^1-N_2)] (**44**) and [{(PPP^{tBu})$(N_2)_2$Mo}$_2$(μ:η^1-η^1-N_2)] (**45**) with weakly activated bridging N_2 were independently reported by *Nishibayashi* and *Mezailles* [99, 100]. They are excellent precatalysts for ammonia generation and N_2 silylation but do not split into nitrides. Starting from nitride **42**, *Mezailles* and

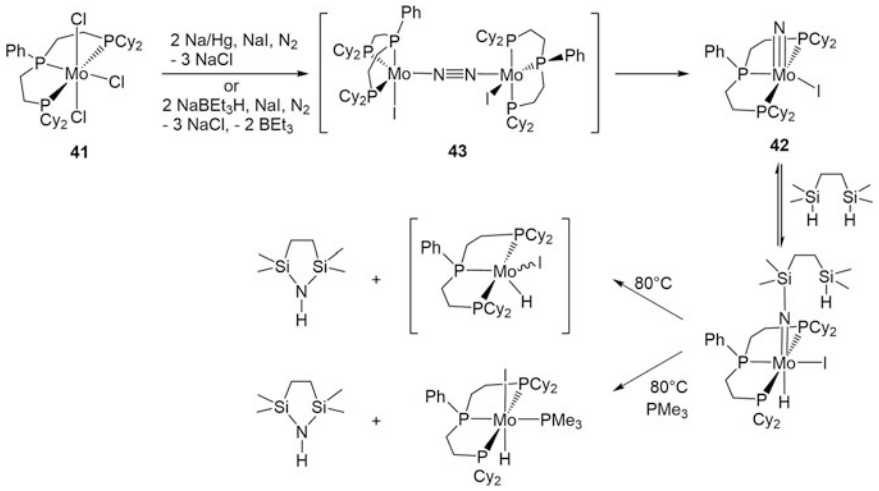

Scheme 14 2 Electron reduction of (PPP)$MoCl_3$ yielding the terminal nitride (PPP)Mo(N)(I) [98]

coworkers were also able to transfer the nitrogen upon metal re-reduction with silanes [98]. Heating with 1,2-bisdimethylsilyethane results in release of the free bis(silyl)amine and presumably reduction of the metal to a molybdenum(II) hydride which was trapped in the presence of PMe_3 as [{Mo^{II}(H)I(PMe_3)(PPP^{tBu})}]. Full regeneration of the metal in terms of a synthetic or even catalytic cycle could not be accomplished so far.

Schneider and coworkers extended this approach beyond group 6. Reduction of the rhenium(III) PNP pincer complexes [$ReCl_2$(PNP)] (**46**, PNP = $N(CH_2CH_2P^tBu_2)_2$) or [$ReCl_3$(PNP)] (**47**) with Na/Hg under N_2 atmosphere gives the rhenium (V) nitride [Re(N)Cl(PNP)] (**48**) in spectroscopic yields up to 90% (Scheme 15) [101, 102]. Alternatively, milder organometallic reductants such as $CoCp^*_2$ can also be used, albeit with slightly lower yield. Intermediates were not detected, but DFT computations supported a mechanism via formation of dinuclear complex [{(PNP)ClRe}$_2$(μ:η^1-η^1-N_2)] (**49**). For this putative intermediate, triplet, open shell singlet (BS[1,1]), and singlet wavefunctions were found close in energy. However, they all resemble the π^{10} configuration expected for such a dimer from the simple symmetry considerations in Scheme 1, again in analogy with *Cummins*' molybdenum triamide and possibly with *Schrock's* and *Mézailles*' pincer systems (see above). Splitting of **49** into **48** was computed to be exergonic by $\Delta G^0 = 98$ kJ mol^{-1} via a zigzag hydrazido transition state with a moderate kinetic barrier ($\Delta G^{\ddagger} = 84$ kJ mol^{-1}). The PNP pincer ligand also features a strongly π-donating dialkylamide group in the ligand backbone. It can overlap with the Re–N–N–Re π-manifold to promote charge transfer to N_2, which requires ligand rotation for the triamide platform where the amide ligands are orthogonal (see above). Starting from nitride **48** the group of *Schneider* also reported nitrogen transfer by formation of acetonitrile within a synthetic cycle, which will be discussed in Sect. 4.

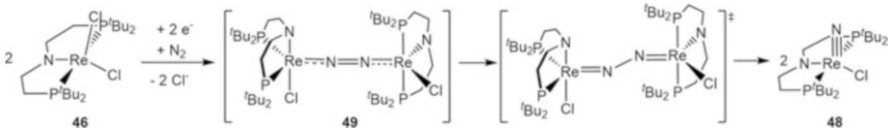

Scheme 15 Proposed N_2-splitting mechanism mediated by a rhenium PNP pincer complex [101]

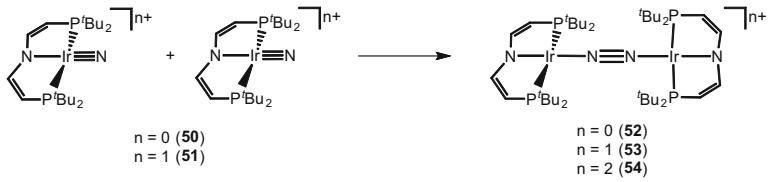

Scheme 16 Coupling of neutral and cationic (PNP)Ir nitrides to (μ-N_2)-complexes [103, 105]

The microscopic reverse, i.e., nitride coupling to N_2, was also examined with pincer complexes, to elucidate the boundaries for the covalent N_2-bonding model [103–105]. *Schneider* and coworkers examined the coupling of the iridium nitrides $[IrN(PNP)]^{n+}$ (n = 0 (**50**), 1 (**51**); PNP = N(CHCHP*t*Bu$_2$)$_2$) to the three possible N_2-bridged dimers of the Ir^I/Ir^{II} redox series $[(PNP)IrN_2Ir(PNP)]^{n+}$ (n = 0 (**52**), 1 (**53**), 2 (**54**)), and structurally characterized them [105] (Scheme 16). From a simple isolobal relationship with octahedral L_5M–N–N–ML_5 complexes (Scheme 1), the square-planar geometry gives rise to π^{12} configuration for Ir^I/Ir^I dimer **52**, π^{11} for mixed-valent Ir^I/Ir^{II} species **53** and π^{10} for dicationic Ir^{II}/Ir^{II} compound **54**, which was qualitatively confirmed by DFT computations. All three coupling reactions were found to be thermodynamically downhill and all proceed via zigzag transition states in analogy to the reverse N_2-splitting. Hence, N_2-splitting of the π^{10} dimer **54** is thermodynamically unfavorable due to weak M–N multiple bonding for late transition metals such as iridium. This observation emphasizes the limitations of the covalent N_2-bonding scheme with respect to N_2-splitting reactivity. However, a decreasing driving force for coupling to dimers **52** ($\Delta G = -102$ kcal/mol), **53** ($\Delta G = -97$ kcal/mol), and **54** ($\Delta G = -74$ kcal/mol) was computed, respectively. This trend in fact reflects the MO picture, as for the π^{11} (**53**) and π^{12} (**52**) dimers the respective iridium(IV) nitride **50** is destabilized by population of antibonding Ir–N π*-MO [103].

3.3 N_2-Splitting by Group 6 Cyclopentadienide Complexes

The end-on bridged dinuclear group 6 dinitrogen complexes [{Cp*M(am)}$_2$(μ-N_2)] (M = Mo (**12**), W (**13**); am = *i*PrNC(Me)N*i*Pr) were prepared by *Sita* and coworkers upon reduction of the respective M^{IV} dichlorides [40]. These diamagnetic

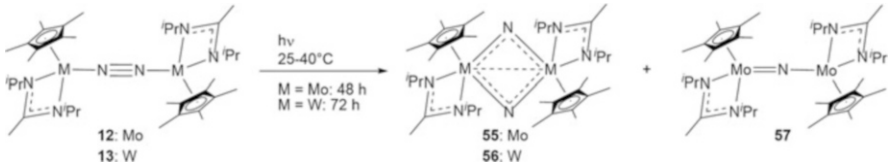

Scheme 17 N_2 cleavage in μ-nitrido and bis(μ-nitrido) complexes by *Sita*'s group [106]

complexes exhibit a π^8 M–N–N–M core with moderate activation and are thermally stable with respect to splitting into nitrides. However, irradiation with a mercury lamp results in splitting of the N–N bond to the dimeric, diamagnetic M^V nitrides $[\{Cp^*M(am)\}_2(\mu\text{-}N)_2]$ (M = Mo (**55**), W (**56**)) and, in case of M = Mo, together with mixed valent Mo^{IV}/Mo^{III} mononitride bridged $[\{Cp^*Mo(am)\}_2(\mu\text{-}N)]$ (**57**) (Scheme 17) [106]. The mechanism of this reaction is not known. However, the product distribution is reminiscent of the photolysis of *Cummins*' trianilide $[\{(ArtBuN)_3Mo\}_2(\mu\text{-}\eta^1\text{:}\eta^1\text{-}N_2)]$ **3** (see Sect. 3.1). There, relaxation of a hot ground state that arises from photoexcitation and internal conversion provides entry to competing N–N and Mo–N cleavage pathways upon coupling with vibrational distortions of the Mo–N–N–Mo core. In the present case, such a mechanism could result in the formation of [Cp*Mo(am)N] and [Cp*Mo(am)] which subsequently dimerize to a statistical mixture of the dinitride and nitride dimers. Importantly, such a mechanism implies the formation of the molybdenum(V) (d^1) nitride from the π^8-dimer. Hence, charge transfer from metal-based d-orbitals to the N_2-ligand required for N–N bond splitting might be possible at least photochemically. This photochemical N_2-splitting reaction was complemented with nitride transfer within a synthetic cycle producing isocyanate with CO_2 and chlorosilane. This reaction is discussed in Sect. 4.

This work is related to the reactivity of a redox series of N_2-bridged dimolybdenum pianostool complexes supported by a ferrocenyldiphosphine ligand. The three complexes $[\{Cp^*Mo(depf)\}_2(\mu\text{-}\eta^1\text{-}\eta^1\text{-}N_2)][BAr^F{}_4]_n$ (n = 0 (**58**), 1 (**59**), 2 (**60**); depf = 1,1′-bisdiethylphosphinoferrocene; Scheme 18) were reported by *Nishibayashi* and *Yoshizawa* [107, 108]. The solution magnetic properties of **60** (diamagnetic), **59** (μ_{eff} = 2.1 μ_B), and **58** (μ_{eff} = 3.2 μ_B) at room temperature in combination with the moderate (**58**: d_{NN} = 1.182(5) Å) to strong (**60**: d_{NN} = 1.256 (9) Å) degrees of N_2 activation support low-spin π^8 (**60**), π^9 (**59**), π^{10} (**58**), configurations, respectively. This is reminiscent of the series **3-5** $[\{(ArtBuN)_3Mo\}_2(\mu\text{-}\eta^1\text{:}\eta^1\text{-}N_2)]^{n+}$ (n = 0–2; see Sect. 3.1) reported by *Cummins*. In analogy, the allegedly least activated N_2 complex **58** splits into nitride $[\{Cp^*Mo^{IV}N(depf)\}_2]$ (**61**) upon irradiation at $400 < \lambda < 580$ nm. TD-DFT computations point towards a transition at λ_{calc} = 495 nm with strong metal to N_2-ligand charge transfer character that might be relevant for the splitting reactivity. Importantly, oxidation of **61** with ferrocenium results in the reverse, i.e., thermal coupling to dinitrogen complex **60**. This inversion of the N_2-splitting/coupling thermochemistry is in line with the electronic configurations of **58** (π^{10}: splitting) and **60** (π^8: coupling), respectively. Interestingly,

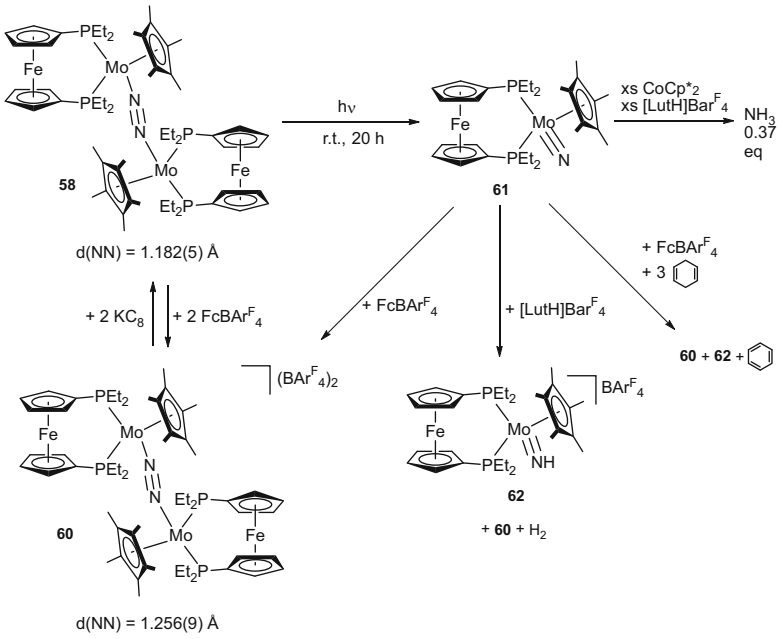

Scheme 18 N_2 cleavage and functionalization mediated by a {Mo(depf)(Cp*)} complex [107]

oxidation of **61** in the presence of the hydrogen atom donor 1,4-cyclohexadiene results in the hydrogen atom transfer product $[\{Cp^*Mo^{IV}(NH)(depf)\}_2]^+$ (**62**) besides nitride coupling, which might give entry into nitride transfer reactivity. Moreover, protonation of **61** gives the same products, but the mechanism for this disproportionation remains unclear.

3.4 N_2-Splitting Beyond Group 7 Elements

Group 8 elements, in particular iron, are the metals used as catalysts for the *Haber-Bosch* process, which in fact proceeds via initial, turnover limiting dissociative N_2 chemisorption. However, despite intense efforts [109–113], for a long time only the reverse reaction of N_2-splitting, i.e., nitride coupling, were known for molecular iron [114–116], ruthenium [117], and osmium [118–122] complexes. Most of these dimerize as octahedral or square-planar M^V nitrides. They are destabilized due to the population of an antibonding M–N π^*-MO, which drives dimerization to the N_2-bridged complexes with π^{12} M–N–N–M cores. The same situation was shown for isolobal, square-planar group 9 M^{IV} (M = Rh, Ir) nitrides, which were examined by *Schneider* and coworkers (see Sect. 3.2). In contrast, the iron(IV) nitride [FeN(BP_3)] ($BP_3^- = PhB(CH_2P\mathit{i}Pr_2)_3^-$) (**63**) also undergoes coupling at room temperature, yet exhibiting an electronic closed-shell ground state. Coupling produces

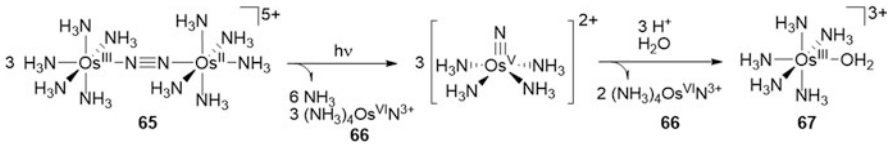

Scheme 19 Photoinduced N_2 cleavage mediated by an osmium complex [123]

[{$(BP_3)Fe$}$_2$(μ-η^1-η^1-N_2)] (**64**) with two exchange-coupled high-spin Fe(I) ions in threefold symmetry bridged by neutral N_2. Analysis of the magnetic data favored this valence state assignment over a three-spin model constituted by two high-spin Fe(II) ions bridged by N_2^{2-} (S = 1). Hence, the metal high-spin state reduces charge transfer to the N_2 ligand resulting in only moderate activation (d_{NN} = 1.138 (6) Å) thereby contributing to the instability of the iron(IV) nitride.

The first report of N_2-cleavage beyond group 6 was reported by *Kunkely* and *Vogler* in 2010. Irradiation of mixed-valent Os^{II}/Os^{III} N_2-complex [{$(NH_3)_5Os$}(μ-η^1-η^1-N_2)]$^{5+}$ (**65**) in acidic aqueous solution was reported to yield osmium(VI) nitride $[OsN(NH_3)_4]^{3+}$ (**66**) and $[Os^{III}(NH_3)_5(H_2O)]^{3+}$ (**67**) (Scheme 19) [123]. The authors proposed a mechanism via photochemical N_2-splitting into Os^{VI} and transient Os^{V} nitrides. The latter disproportionates with subsequent hydrolysis forming ammonia with an overall yield of 16%.

Shortly after, *Holland* and coworkers presented the first example of N_2-splitting to a well-defined molecular iron nitride complex. Reduction of the dimeric iron(II) β-diketiminate complex $[FeCl(L)]_2$ (L = MeC[C(Me)N(2,6-$Me_2C_6H_3$)]$_2$) (**68**) with KC_8 under N_2 affords the isolation of the remarkable dinitride complex K_2[{Fe(L)}$_4$(μ-N)$_2$(μ-Cl)$_2$] (**69**) (Scheme 20) upon full scission of the N–N bond (d_{NN} = 2.799(2) Å) [124]. NMR studies indicate that the complex, multinuclear structure is maintained in solution. Mössbauer spectra suggest the valence assignments as two high-spin Fe^{II} and two high-spin Fe^{III} ions, in agreement with the overall charge balance for 6-electron N_2 reduction. The cooperativity of four iron centers avoids the unfavorable formation of high-valent iron. Previous work from that group emphasizes the strong influence of subtle ligand variations. Reduction of the mononuclear β-diketiminate complex [(L')FeCl] (L' = HC[C(^{t}Bu)N(2,6-^{i}$Pr_2C_6H_3$)]$_2$) (**70**) yields N_2-bridged K_2[{(L')Fe}$_2$(μ-η^1-η^1-N_2)] (**71**), which exhibits strong N_2-activation (d_{NN} = 1.23 Å, υ_{NN} = 1,589 cm^{-1}) but does not split into nitrides [125]. This difference was attributed to ligand sterics, which prevent nitride stabilization by cluster formation in the latter case. Computational analysis for **68** suggested initial formation of a Fe–N–N–Fe core followed by side-on coordination of a third Fe(I) fragment for the smaller ligand [126]. After structural rearrangement to a side-on/side-on/end-on conformation, coordination of the fourth iron fragment leads to N–N cleavage. This study and subsequent experimental work emphasized an important influence of the alkaline cation in stabilizing the nitride cluster and enabling N_2-splitting [127, 128]. Splitting is reversible as demonstrated by addition of the strong π-acceptor CO, which results in N_2 reductive elimination

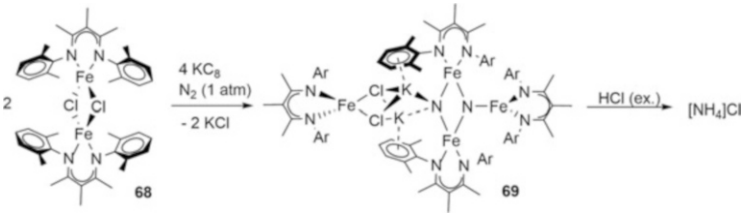

Scheme 20 N_2 cleavage and ammonia formation mediated by a dinuclear iron compound [124]

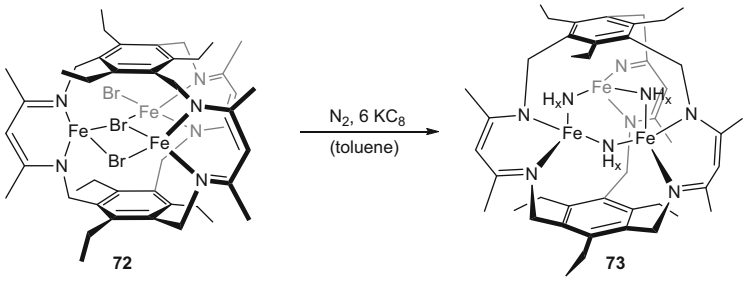

Scheme 21 N_2 cleavage by a designed trinuclear Fe complex [132]

[129]. Addition of several acids to **68** yields ammonia in up to 96% yield [130]. An impressive number of intermediates could be isolated for the protonolysis, giving insights into a potential mechanism for ammonia formation. They also illustrate the strong basicity of the system and the strong reductants that are required for stepwise reduction/protonation can be offset by proton-coupled electron transfer reactions. Removal of the supporting potassium ion in **68** by addition of 18-crown-6 reveals a very basic nitrogen moiety, which ends up in intramolecular C–H activation of a benzylic CH_3 group of the ancillary ligand to form N–H bonds [131]. Strong nucleophilicity of the unmasked nitride is also displayed by C–N bond formation with methyl tosylate resulting in a bridging imide/nitride.

Murray and coworkers used a multimetallic, cooperative approach to split N_2 upon reduction of a triiron(II) complex **72** with KC_8 (Scheme 21) [132]. The three Fe ions in the main product **73** were found to bridge through three NH_x functions. Mössbauer spectra show the presence of localized triiron(II/II/III) at low temperatures. The presence of three nitrogen atoms per cluster suggests intra- and intermolecular cooperativity. The origin of the hydrogen atoms in the bridging NH_x moieties could not be determined so far. Reaction in silylated glassware, deuterium labeling experiments, and addition of compounds with weak C–H bonds (9,10-dihydroanthracene) did not give a satisfactory explanation. Addition of HCl to this compound yields about 30% ammonia, indicating that only one of three nitrogen units can be liberated in this way.

4 Nitride Functionalization Following N_2-Splitting

The reactivity of transition metal nitrides, as depending on the metal type and oxidation state, was extensively examined and summarized in several comprehensive review articles [11, 133, 134]. Nitride ligands mostly exhibit nucleophilic reactivity except for some examples of high-valent late transition metal nitride complexes (Ru, Os, Ir). Accordingly, the reactivity of nitrides that originated from N_2-splitting with electrophiles was examined. Several groups reported the generation of ammonia upon protonolysis of well-defined N_2-derived nitride complexes. Concerning group 6-8 metals the reports by the groups of *Budzelaar* (Cr) [96], *Nishibayashi* (Mo) [107], *Vogler* (Os) [123], *Holland* (Fe) [113, 124], and *Murray* (Fe) [132] were already presented in the preceding section. Besides these, further examples from *Chirik* (Ti) [63], *Hou* (Ti) [135], *Gambarotta* (Ti and V) [136, 137], *Kawaguchi* (Nb) [138], and *Mindiola* (Nb) [139] using early transition metals are also known. However, the generation of ammonia is not in the main focus of this review. Instead, in this section the transfer of nitrogen from N_2 by N–C bond formation via initial N_2-splitting will be discussed. When considering possible target molecules for the synthesis of organics with N_2 as nitrogen source it is instructive to assess the thermochemistry of hypothetical reactions. *Caulton* and coworkers discussed several reactions where N_2 is incorporated into organic molecules with retention of one or two N–N bonds (selected reactions in Scheme 22) [140]. With high energy starting materials like acetylenes and N-heterocycles as synthetic targets, particularly when stabilized by aromaticity, several

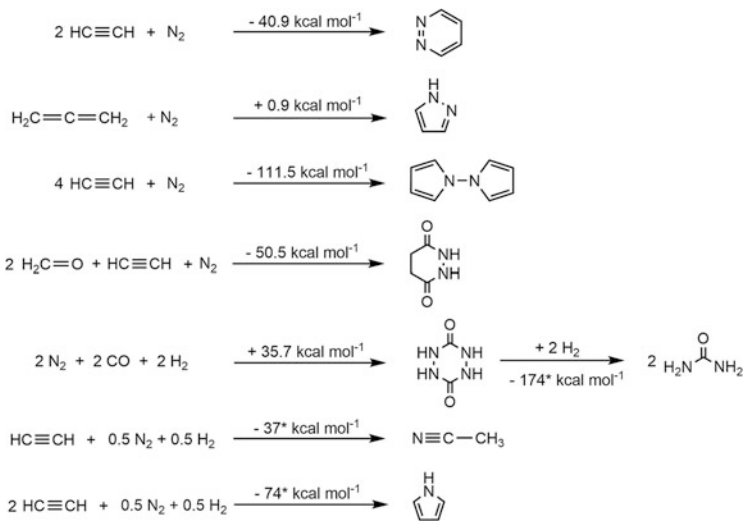

Scheme 22 Computed reaction enthalpies ΔH_r for N_2 functionalization from *Caulton* and coworkers [140] (numbers marked with * are experimental values for gas phase reactions retrieved from Ref. [142])

thermodynamically accessible reactions were pointed out. In addition, formation of strong C=N (e.g., heterocummulenes) or C≡N (nitriles) bonds can offset the high energy demand for complete N_2 cleavage [141]. For example the C≡N bond dissociation energy (D^0(HC≡N) = 937 kJ mol^{-1}) is close to that of N_2 providing a driving force for catalytic transformations of N_2 to nitriles. Unfavorable reactions can be turned exothermic by simultaneous hydrogenation. Besides, H_2 can serve as attractive mild reductant for nitrogen.

4.1 Formation of Heterocummulenes

The group of *Kawaguchi* demonstrated N_2 cleavage upon reaction of a Nb(V) dichloride with a chelating triphenoxide ligand with $LiHBEt_3$ (6 eq.) [143]. Subsequent work with a related triphenoxy ligand gave further insights into the mechanism (Scheme 23). The (μ-H)$_4$-bridged dimer $K_2[(L^{OPh3}Nb^{IV})_2(\mu\text{-H})_4]$ (**74**) directly reacts with N_2 upon H_2 elimination and N–N bond cleavage to the bis(μ-nitrido) complex $K_2[(L^{OPh3}Nb)_2(\mu\text{-N})_2]$ (**75**; L^{OPh3} = HC-*o*-(C_6H_2O-4,6-tBu_2)$_3$) [138]. Within a series of stoichiometric reactions, this compound could be transformed to a mononuclear ureate complex via nitride alkylation, dimer cleavage with pyridine and oxo/imido-metathesis with CO_2 [144]. Importantly, the immediate product from N_2-splitting does not react with CO_2, presumably because of low nucleophilicity of the bridging nitride and steric bulk. Ureate formation from the imide intermediate is proposed to proceed via initial [2 + 2] addition of CO_2 and subsequent extrusion of methyl isocyanate. Besides the dimeric oxo complex, the ureate would then result from MeNCO addition to another parent imido complex. However, reaction intermediates or free MeNCO could not be detected. Liberation of free heterocummulenes like isocyanate or carbodiimide or of dimethylurea was not reported.

The same group later established a full synthetic cycle for isocyanate from N_2 formation with a related system. Reduction of vanadium complex $[(ONO)V^{III}(THF)]$ (ONO = 2,6-(3-^{t}Bu-5-Me-2-$OC_6H_2CH_2$)-4-^{t}Bu-(p-tolyl)NC_6H_4) (**76**) with KH (2 equiv) under N_2 atmosphere gives the nitride bridged $[\{K(DME)\}_2\{(ONO)V^{IV}(\mu\text{-N})\}]_2$ (**77**) in 61% yield (Scheme 24) [145]. Oxidation with benzoquinone affords the terminal vanadium(V) nitride $K[(ONO)V^VN]$ (**78**). Regeneration of the V^{IV} nitride dimer with KH was not successful, suggesting that the V^V nitride is not an intermediate in N_2-splitting. Nitrogen atom transfer to CO or isonitriles was accomplished, generating the respective vanadium(III) isocyanate (**79**) and carbodiimide (**80**) complexes. After C–N bond formation free potassium isocyanate precipitates in toluene upon trapping the alkyne complex [(ONO)V(η^2-MeCCMe)] (**81**) with dimethylacetylene. From there, parent **76** could be regenerated by dissolving **81** in THF.

A full synthetic cycle to isocyanates from N_2 could also be established by *Sita* and coworkers [106]. Earlier work of this group demonstrated thermal N_2-splitting for the N_2-bridged group 5 complexes $[\{Cp^*(am)M\}_2(\mu{:}\eta^1\text{-}\eta^1\text{-}N_2)]$ (M = Nb (**10**),

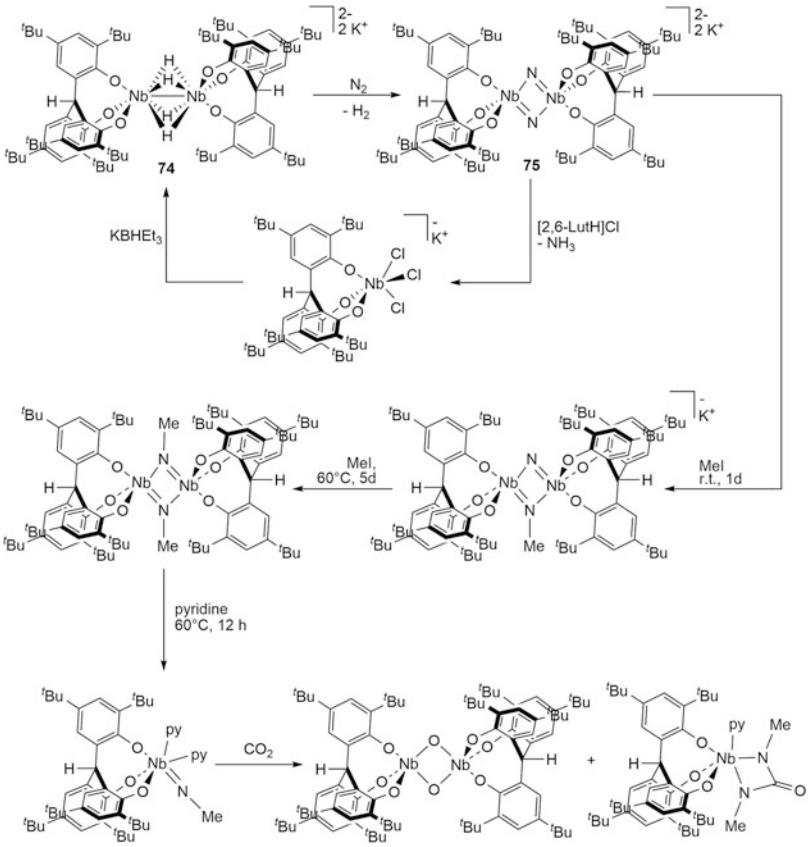

Scheme 23 N_2-splitting by a Nb hydrido complex and functionalization of the resulting bis (μ-nitrido) [138, 144]

Ta (**11**); Scheme 25, top), which exhibit strong N_2 activation in the ground state (see Sect. 2.2) [39, 41]. Functionalization of the tantalum nitride was achieved by N–Si bond formation with silanes [39], reminiscent of work by the group of *Mézailles* (c.f. Sect. 3.2). This approach could be transferred to the analogous group 6 system. Photolysis of [{Cp*(am)M}$_2$(μ:η^1-η^1-N_2)] (M = Mo (**12**), W (**13**)) yields nitride-bridged dinuclear complexes **55** and **56** (c.f. Sect. 3.3) [40]. Addition of R_3ECl (R_3E = Me_3Si, Ph_3Si, Me_3Ge, Me_3C) to the bis(μ-nitrido) complexes **55** and **56** produces a 1:1 mixture of the mononuclear nitride [Cp*M(am)M(N)Cl] and the imide [Cp*M(am)(N-ER_3)] (**82**). A radical mechanism was proposed. In contrast, irradiation of **12** or **13** in the presence of Me_3SiCl gives the imide complex **82** and dichloride [Cp*M(am)Cl_2] (**83**) in 2:1 ratio (Scheme 25, bottom). Reaction of the imide with CO affords free silylisocyanate in up to 64% yield and the bis(carbonyl) complex [Cp*M(am)$(CO)_2$] [106, 146]. To close the synthetic cycle, the latter complexes could be converted to the respective dichlorides **83** either by reaction

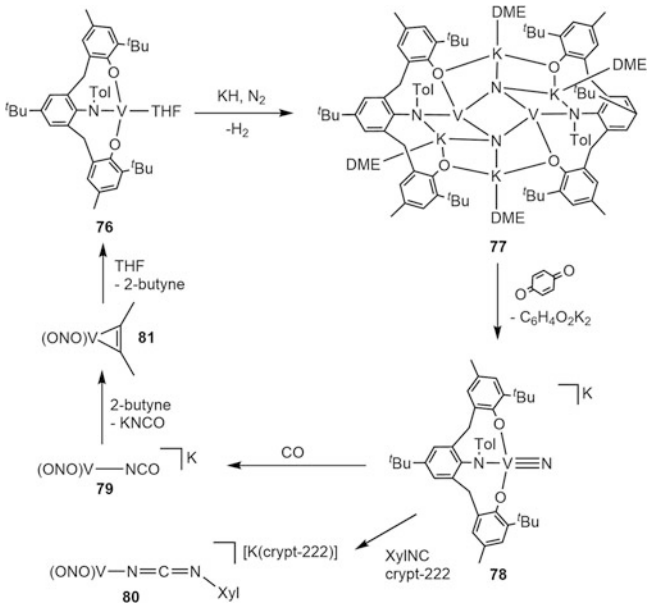

Scheme 24 Synthetic cycle for N_2 to isocyanate conversion promoted by vanadium complexes [145]

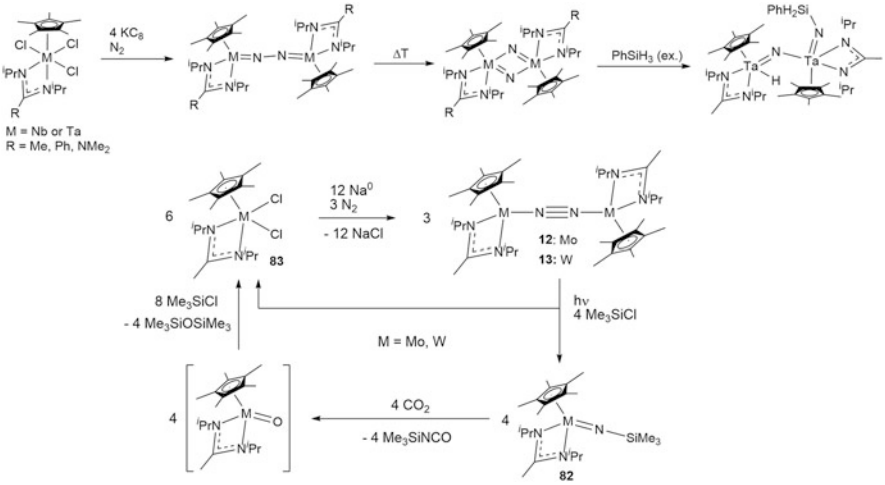

Scheme 25 N_2-splitting and functionalization mediated by group 5 complexes (*top*, [39]) and a synthetic cycle for N_2 to isocyanate conversion by group 6 metal complexes (*bottom*, [146])

with CO_2 and subsequent treatment of the resulting oxo complex with Me_3SiCl or directly by reaction of the silylimide under CO_2 (1.4–4.8 bar) in the presence of Me_3SiCl (Scheme 25). On this route, free isocyanate could be generated from N_2 in

a pseudo-catalytic, four step one-pot synthesis with up to 82% recovered catalyst per cycle.

Attempts to get isocyanates from the reaction of CO with *Cummins*' molybdenum(VI) nitride [MoN(N*t*BuAr)$_3$], which results from N_2-splitting failed [147]. While DFT computations predicted that this reaction should be thermodynamically possible, a large kinetic barrier presumably arises from the lack of a carbonyl complex intermediate that can rearrange to an isocyanate. In comparison, this pathway was computationally proposed for a related vanadium(V) nitride, which forms isocyanates with CO, but which is not derived from N_2 [147–149].

4.2 *Formation of Nitriles*

Nitriles represent another synthetic target that was addressed by several groups using molybdenum (*Cummins*), rhenium (*Schneider*), and titanium (*Hou*) platforms. Seminal work in this area was reported by *Cummins* and coworkers starting from the trisanilide molybdenum(VI) nitrides that arise from N_2-splitting (c.f. Sect. 3.1). [Mo(N)(N*t*BuAr)$_3$] (**27**) exhibits only weak nucleophilicity but can be activated with strong Lewis acids, including alkylation, silylation, and acylation with MeOTf, Me_3SiOTf, or in situ prepared PhC(O)OTf, respectively [150]. The methylimido complex **84** can be deprotonated (Scheme 26). The resulting ketimide **85**, with approximately linear Mo=N=CH_2 unit, is a *C*-nucleophile giving the ethylimide [Mo(NEt)(N*t*BuAr)$_3$]$^+$ **86** with MeI. Interestingly, the ethylimide could not be obtained by direct ethylation of the nitride with EtOTf, EtI, or [Et_3O]BF_4, respectively [150]. As an extension of this work, *Cummins* later reported the formation of a cyanide complex from nitride **27** (Scheme 26). With a mixture of $MeOCH_2Cl$ and $^iPr_3SiOTf$ a methoxymethylimide complex **87** was obtained and deprotonation leads to the respective alkoxyketimide [Mo(NCHOMe)(N*t*BuAr)$_3$] (**88**) [151]. Release of free prussic acid with Lewis acid was not successful, but a mixture of Lewis acid/Brønsted base ($SnCl_2$/Me_3SiNMe_2) gave the molybdenum (IV) cyanide complex [Mo(CN)(N*t*BuAr)$_3$] (**89**). While this approach of

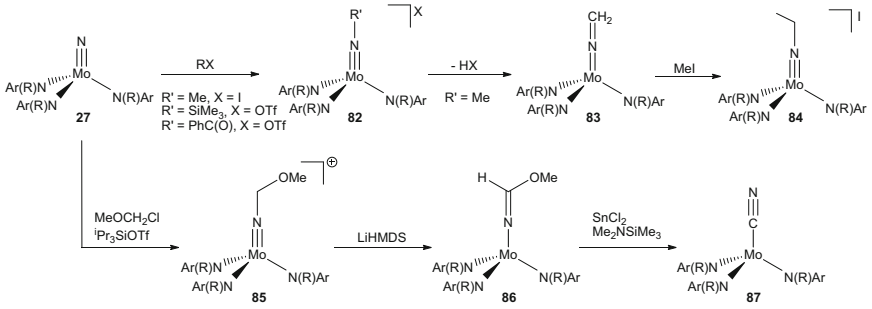

Scheme 26 Functionalization of N_2-derived terminal nitrido complex 27 with electrophiles

N_2-functionalization via splitting, alkylation, and ligand oxidation processes did not lead to pseudo-catalytic synthetic cycles or even catalysis with this system yet, it is conceptually relevant concerning the redox-balance. It demonstrates that metal -re-reduction, in this case Mo^{VI} to Mo^{IV}, can at least in part be accomplished without external reducing equivalents, but through a charge transfer from the ligand to metal that is coupled with imide deprotonation. In fact, deprotonation of alkylimides to ketimides and even double deprotonation to nitriles – a formal transfer of four electrons to the metal – were well known but previously not applied to N_2 functionalization [152, 153]. This approach was later also picked up by *Schneider* and coworkers to establish a full synthetic cycle for nitrile generation from N_2 (see below).

De Vries and coworkers were the first ones to transfer the N_2-derived nitride from *Cummins'* system to an organic compound. Reaction of **27** with trifluoroacetic anhydride in DMF results in release of free amide $CF_3C(O)NH_2$ in high yield with respect to nitrogen [154]. However, the molybdenum trisanilide platform is degraded and, in fact, the *tert*-butylamide groups serve as proton source, preventing catalytic turnover. An elegant route for full nitrogen transfer starting from **27** was provided by *Cummins* in 2006 [155]. Acylation with $RC(O)Cl/SiMe_3OTf$ (R = Ph, ^{t}Bu, Me) gives the respective acylimide complexes **90** (Scheme 27). These can be reduced with Mg/anthracene in the presence of Me_3SiCl to a trimethylsiloxy-ketimide **91**. Salt metathesis with Lewis acids like $SnCl_2$ or $ZnCl_2$ results in fragmentation to the free organonitrile and molybdenum(IV) chloride [MoCl(N*t*BuAr)$_3$] (**92**). Further reduction restores the parent Mo^{III} triamide. In this synthetic cycle, nitriles were produced in up to 38% yield over all steps. Each molybdenum center is oxidized by 3 electrons upon N_2 cleavage and re-reduction is a purely metal centered process.

This system was later extended to heterobimetallic (Mo/Nb) N_2-cleavage and -functionalization. N_2-bridged (π^9-electron) complex [(Ar^{t}BuN)$_3$Mo(μ-η^1-η^1-N_2)Nb(N^{i}PrAr)$_3$] (**93**) splits into Mo^{VI} nitride **27** and Nb^V nitride [NbN(N^{i}PrAr)$_3$]$^-$

Scheme 27 Synthetic cycle for N_2 cleavage and conversion to nitriles [155]

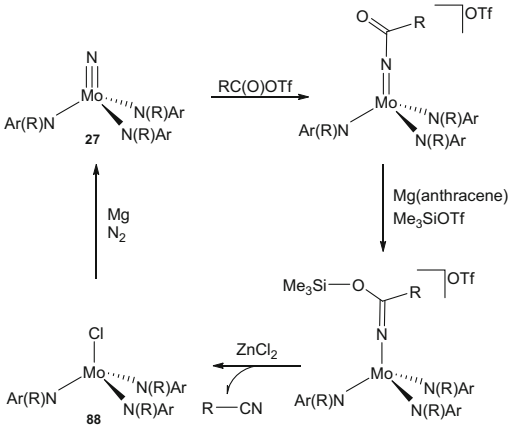

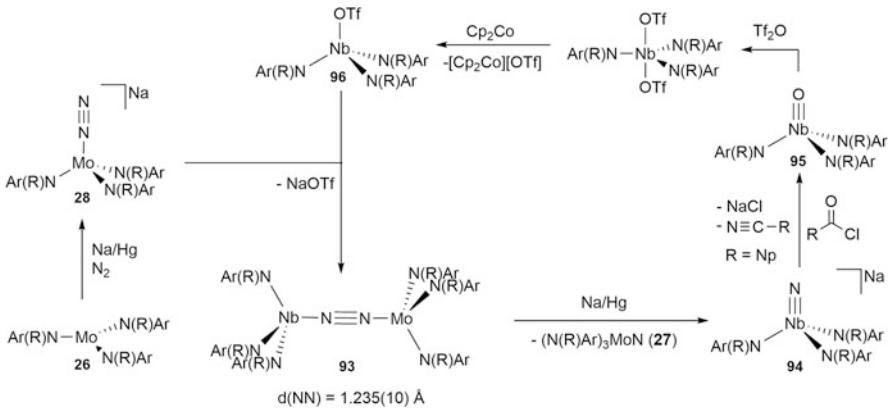

Scheme 28 Synthetic cycle for N_2 to organonitrile conversion mediated by a heterobimetallic Nb/Mo system [156, 157]

(**94**) upon reduction (Scheme 28) [156]. This nitrido niobate is more reactive than the isoelectronic Mo complex. With acyl chlorides, unusual oxo/nitride metathesis is observed directly producing the free nitrile and the Nb^V oxo complex (**95**) [157]. Closing of the cycle with respect to niobium was accomplished by addition of trifluoromethanesulfonic anhydride, reduction with $CoCp_2$ and metathesis of the Nb^{IV} triflate **96** with $[(N_2)Mo(N^tBuAr)_3]^-$ **28**. Ligand modification allowed for trapping of an Nb^V acylimido complex, which converts into the oxo-complex upon heating. A variety of nitriles can be synthesized in high yield, providing the opportunity of selective, atom-efficient ^{15}N-labelling employing $^{15}N_2$. However, while this synthetic cycle is pseudo-catalytic in Nb it is still stoichiometric in Mo.

Related work was reported by *Hou* and coworkers with a titanium cyclopentadienide platform, which even enabled the use of H_2 as reductant for N_2-cleavage. (Scheme 29) [135, 158]. Hydrogenolysis of the titanium(IV) alkyl complex [Cp´Ti$(CH_2SiMe_3)_3$] (Cp´ = $C_5Me_4SiMe_3$) (**97**) with dihydrogen (4 atm) affords a mixture of the partially reduced, mixed-valent, trinuclear polyhydride [(Cp´Ti)$_3(\mu_3\text{-H})(\mu_2\text{-H})_6$] (**98**: 69%) and [(Cp´Ti)$_4(\mu\text{-H})_8$] (10%, not shown in Scheme 29). [(Cp´M)$_4(\mu\text{-H})_8$] is the main product in case of homologous Zr and Hf [159]. However, only **98** reacts with N_2 (1 atm) upon partial H_2 elimination and formation of [(Cp´Ti)$_3(\mu_2\text{-NH})(\mu_3\text{-N})(\mu_2\text{-H})_2$] (**99**) with full N_2-cleavage and retention of the formal metal oxidation states {Ti^{III}_2/Ti^{IV}}. The side-on end-on N_2-bridged complex [(Cp´Ti)$_3(\mu\text{-}\eta^1\text{:}\eta^2\text{-}\eta^2\text{-N}_2)(\mu\text{-H})_3$] was spectroscopically identified as an intermediate at −30°C. Above −10°C, N_2-splitting is observed to the bis-μ-nitride [(Cp´Ti)$_3(\mu_3\text{-N})(\mu_2\text{-N})(\mu_2\text{-H})_3$], which isomerizes to the final product at 20°C. Further N_2-incorporation was observed upon prolonged heating as solid at 180°C. Importantly, direct reaction of [Cp´Ti$(CH_2SiMe_3)_3$] under H_2 (4 atm) and N_2 (1 atm) at 60°C gives the bisimide complex [(Cp´Ti)$_3(\mu_3\text{-NH})_2(\mu_2\text{-H})_4$] (**100**) in 90% yield. Heating of the latter under N_2 (180°C, neat) also results in more N_2-incorportation to the diimide dinitride complex [(Cp′Ti)$_4(\mu^3\text{-NH})_2(\mu^3\text{-N})_2$] (**101**) in about 95%

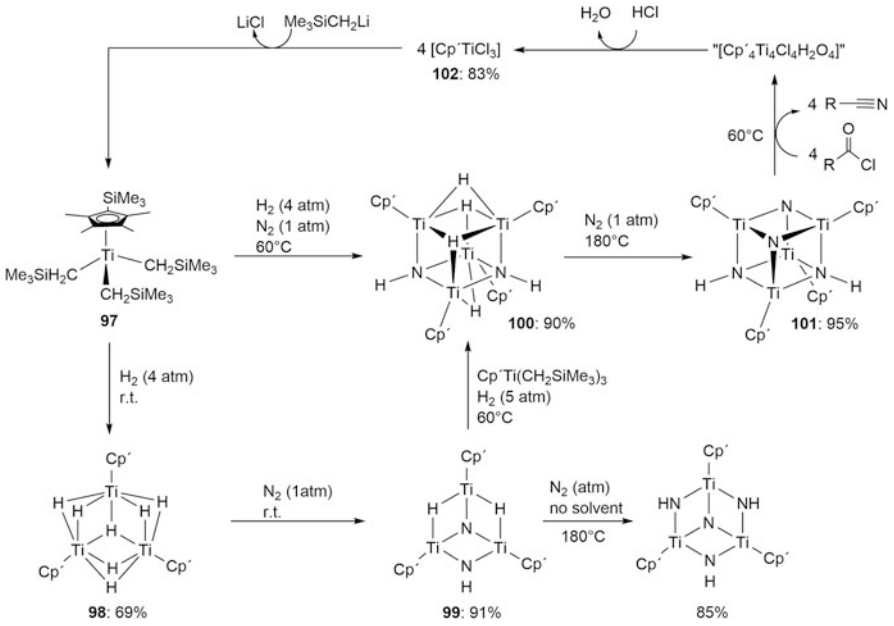

Scheme 29 N_2 functionalization via polynuclear titanium hydrides [135, 160]

yield (Scheme 29) [160]. This complex directly forms a variety of organic nitriles in good yields (60–85%) with acyl chlorides (60°C, 12 h) allowing for nitrogen transfer from N_2 into organic substrates in two simple reaction steps. The μ-oxo complex $[(Cp'TiCl_2)_2(\mu\text{-}O)]$ and several unidentified paramagnetic titanium species also result, which can be recovered as $[Cp'TiCl_3]$ (**102**) in 83% yield upon addition of ethereal HCl to the crude mixture. This enabled a full synthetic cycle by salt metathesis with lithium neosyl. Most importantly, this system does not require strong reductants like alkali metals.

Schneider and coworkers also reported the formation of acetonitrile with N_2 as nitrogen source within a synthetic cycle based on their rhenium pincer platform (Scheme 30). The nitride [Re(N)Cl(PNP)] (**48**, PNP = $N(CH_2CH_2P\textit{t}Bu_2)_2$), which results from N_2-splitting (c.f. Sect. 3.2), does not react with H_2 (3 bar) in contrast with the related square-planar group 8 compounds [M(N)(PNP)] (M = Ru, Os) that form ammonia in high yield [161, 162]. This lack of reactivity was attributed to the strong *trans*-effect of the nitride ligand, which prevents H_2 heterolysis in *trans*-position. However, **48** can be N-alkylated by strong electrophiles, such as alkyltriflates ROTf (R = Me, Et) to the respective imido complexes $[Re(NR)Cl(PNP)]^+$ [102]. In contrast, with Brønsted acids protonation at the amide instead of the nitride nitrogen is observed. The different selectivity follows the computed thermochemical preference for reaction with protons and *C*-nucleophiles, respectively. *Caulton* and coworkers reported similar findings for a ruthenium(IV) nitride that was obtained with azide as nitrogen source [163]. Deprotonation of ethylimide $[Re(NEt)Cl(PNP)]^+$ (**103**) gives the respective ketimide [Re(N=CHMe)Cl(PNP)]

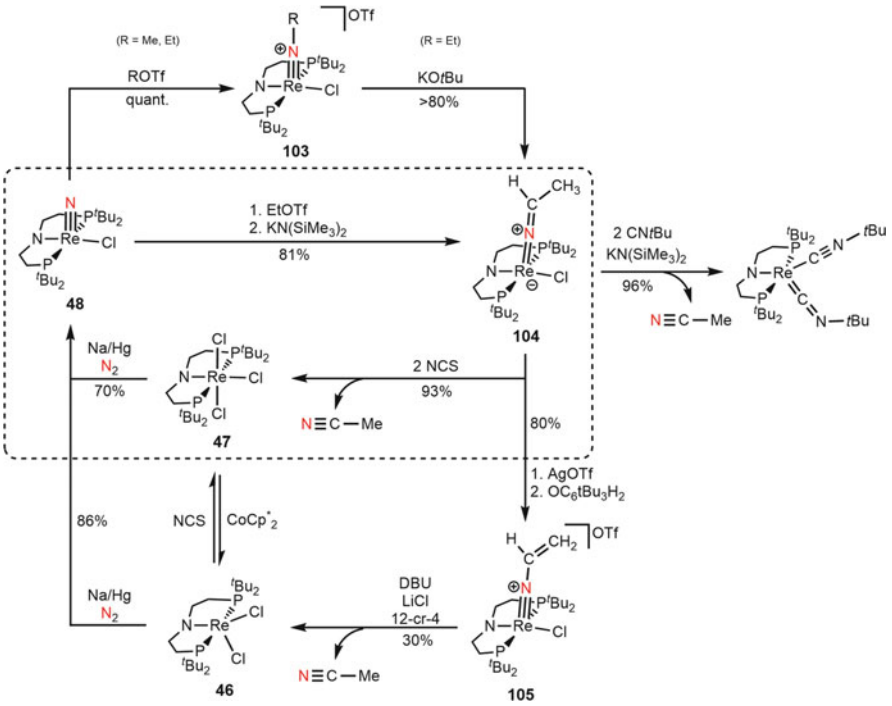

Scheme 30 Synthetic cycle for N_2 to acetonitrile conversion mediated by rhenium PNP pincer complex (DBU = 1,8-Diazabicyclo[5.4.0]undec-7-en, NCS = *N*-chlorosuccinimide). The *dashed box* describes the most efficient cycle [102]

(**104**) in near quantitative yield. The Re–N (1.822(4) Å) and C=N (1.273(7) Å) bond distances and near linearity indicate strong 1-azavinylidene Re=N=C heterocummulene character, also explaining the observation of two stereoisomers of **104**. The formation of **104** directly from the nitride can also be carried out in a two-step, one-pot synthesis. Previous work on other group 6 and group 7 alkylimides that were not derived from N_2 suggests the formation of nitriles (M ← N≡CR) upon double deprotonation of primary alkylimides (M=N–CH_2R) via ketimido (M–N=CHR) intermediates [152, 153]. Both deprotonation steps also represent formal 2-electron reductions of the metal. Hence, this route implies intramolecular proton coupled metal reduction, instead of the use of external reductants used in the protocols of *Cummins* (Mg/anthracene) and *Hou* (H_2), respectively. Deprotonation of **104** was possible upon trapping of the resulting rhenium(I) species with strong π-acceptor ligands, like isonitriles, with concomitant free acetonitrile release in near quantitative yield. Alternatively, external oxidants can be used to avoid the need for additional π-accepting ligands. Net $2e^-/H^+$ removal by stepwise, one-pot oxidation with Ag^+ and subsequent hydrogen atom abstraction with tri-*tert*-butylphenoxy radical gave the vinylimide [Re(NCHCH_2)Cl (PNP)]$^+$ (**105**) in high yield. The preference of the Re^V vinylimido vs. the Re^{III}

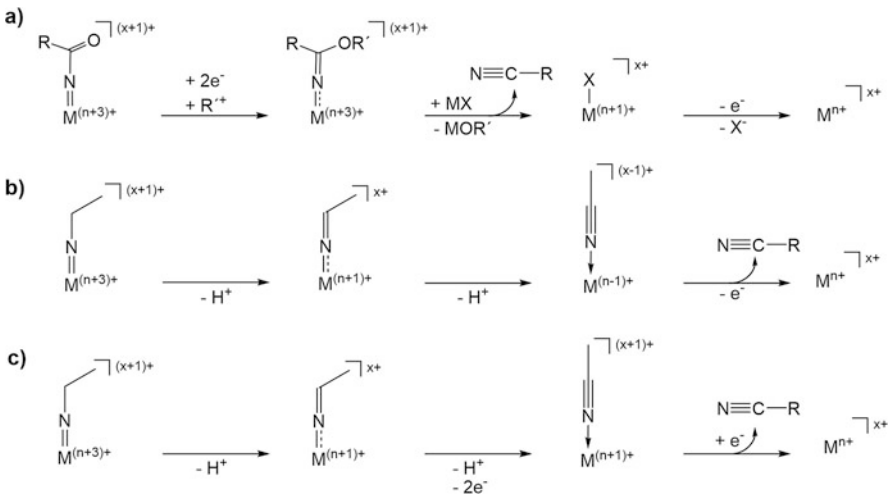

Scheme 31 Schematic pathways of nitrile synthesis after functionalization of N_2-derived nitrides: Nitride acylation (**a**) and alkylation (**b**, **c**) [102]

nitrile complex tautomer emphasizes the electron rich nature of the {Re(PNP)}-platform. However, release of free acetonitrile from **105** is possible by adding a chloride source with catalytic amounts of base (DBU) for tautomerization, albeit in moderate yields. The most efficient route for acetonitrile release from ketimide **104** was obtained using N-chlorosuccinimide (NCS) as combined oxidant, chloride source and base, giving free MeCN and rhenium(IV) chloride [$ReCl_3$(PNP)] **47** in over 90% yield. Versatile reduction of **47** closes a full synthetic cycle.

In comparing the synthetic strategies of the three nitrile protocols discussed above it is instructive to assess the overall redox economy. Both *Cummins* (Mo, Mo/Nb) and *Hou* (Ti) used organic acyl electrophiles for C–N bond formation. Hence, a full cycle comprising N_2-splitting and N-transfer further requires three electrons per *N*-atom for re-reduction of the metal (Scheme 31a). This can be accomplished with external chemical reductants, like electropositive metals (*Cummins*) or H_2 (*Hou*). In contrast, the strategy evaluated by *Schneider* and coworkers relies on intramolecular proton-coupled ligand-to-metal charge transfer. Each deprotonation step is associated with formal 2-electron reduction of the metal. Odd electron N_2 reduction ($3e^-$ per N-atom) requires additional reductive or oxidative redox steps for (pseudo)catalytic turnover (Scheme 31b and c).

5 Conclusions

In this tutorial review, the electronic structures of the most common end-on and side-on bridging N_2-complexes and the parameters that determine splitting into nitrides were discussed. Some general trends such as increasing N_2-activation of the

heavier metal homologues due to better orbital overlap are apparent. Importantly, dinuclear N_2-complexes with π^{10} (end-on) and $\pi^8\delta^2$ (side-on) electrons within the M_2N_2 core, respectively, were pointed out as preferred electronic configurations for splitting into nitrides. Several other parameters, such as π-donating auxiliar ligands, steric influences, high/low-spin transitions, and decreasing M≡N bond strengths along the transition series complicate this simplified picture. However, it provides a good starting point in future efforts to design catalyst platforms that functionalize N_2 via splitting into nitrides. For nitride functionalization that follows N_2-splitting, several synthetic targets were pointed out that could offset cleavage of the strong N_2 bond, such as nitriles, heterocycles, or heterocummulenes. Catalytic protocols that proceed through N_2-splitting are yet to be developed. However, several stoichiometric and pseudo-catalytic variants offer possible solutions to combine C–N bond formation and 6-electron redox reactivity and open up a path towards catalytic N_2 functionalization beyond ammonia in the future.

References

1. Hoffman BM, Dean DR, Seefeldt LC (2009) Climbing nitrogenase: toward a mechanism of enzymatic nitrogen fixation. Acc Chem Res 42:609–619. doi:10.1021/ar8002128
2. Hoffman BM, Lukoyanov D, Yang ZY, Dean DR, Seefeldt LC (2014) Mechanism of nitrogen fixation by nitrogenase: the next stage. Chem Rev 114:4041–4062. doi:10.1021/cr400641x
3. Haber F (1910) Über die Darstellung des Ammoniaks aus Stickstoff und Wasserstoff. Z Elektrochem Angew Phys Chem 16:244–246. doi:10.1002/bbpc.19100160709
4. Ertl G (2008) Reactions at surfaces: from atoms to complexity (nobel lecture). Angew Chem Int Ed 47:3524–3535. doi:10.1002/anie.200800480
5. Bezdek MJ, Chirik PJ (2016) Expanding boundaries: N_2 cleavage and functionalization beyond early transition metals. Angew Chem Int Ed 55:7892–7896. doi:10.1002/anie.201603142
6. Yandulov DV, Schrock RR (2003) Catalytic reduction of dintrogen to ammonia at a single molybdenum center. Science 301:76–78. doi:10.1126/science.1085326
7. Arashiba K, Miyake Y, Nishibayashi Y (2011) A molybdenum complex bearing PNP-type pincer ligands leads to the catalytic reduction of dinitrogen into ammonia. Nat Chem 3:120–125. doi:10.1038/nchem.906
8. Anderson JS, Rittle J, Peters JC (2013) Catalytic conversion of nitrogen to ammonia by an iron model complex. Nature 501:84–87. doi:10.1038/nature12435
9. van der Ham CJM, Koper MTM, Hetterscheid DGH (2014) Challenges in reduction of dinitrogen by proton and electron transfer. Chem Soc Rev 43:5183–5191. doi:10.1039/c4cs00085d
10. Ali M, Zhou F, Chen K, Kotzur C, Xiao C, Bourgeois L, Zhang X, MacFarlane DR (2016) Nanostructured photoelectrochemical solar cell for nitrogen reduction using plasmon-enhanced black silicon. Nat Commun 7:11335. doi:10.1038/ncomms11335
11. Smith JM (2014) Reactive transition metal nitride complexes. In: Karlin KD (ed) Progress in inorganic chemistry, vol 58. Wiley, Hoboken, pp 417–470. doi: 10.1002/9781118792797.ch06
12. Hidai M (1999) Chemical nitrogen fixation by molybdenum and tungsten complexes. Coord Chem Rev 185–186:99–108. doi:10.1016/s0010-8545(98)00250-1
13. Sellmann D (1974) Dinitrogen-transition metal complexes: synthesis, properties, and significance. Angew Chem Int Ed Engl 13:639–649. doi:10.1002/anie.197406391

14. Bazhenova TA, Shilov AE (1995) Nitrogen fixation in solution. Coord Chem Rev 144:69–145. doi:10.1016/0010-8545(95)01139-g
15. Jia HP, Quadrelli EA (2014) Mechanistic aspects of dinitrogen cleavage and hydrogenation to produce ammonia in catalysis and organometallic chemistry: relevance of metal hydride bonds and dihydrogen. Chem Soc Rev 43:547–564. doi:10.1039/c3cs60206k
16. Shilov AE (2003) Catalytic reduction of molecular nitrogen in solutions. Russ Chem Bull 52:2555–2562. doi:10.1023/b:rucb.0000019873.81002.60
17. Fryzuk MD, Johnson SA (2000) The continuing story of dinitrogen activation. Coord Chem Rev 200–202:379–409. doi:10.1016/s0010-8545(00)00264-2
18. MacKay BA, Fryzuk MD (2004) Dinitrogen coordination chemistry: on the biomimetic borderlands. Chem Rev 104:385–401. doi:10.1021/cr020610c
19. Badger RM (1934) A relation between internuclear distances and bond force constants. J Chem Phys 2:128–131. doi:10.1063/1.1749433
20. Evans WJ, Fang M, Zucchi GL, Furche F, Ziller JW, Hoekstra RM, Zink JI (2009) Isolation of dysprosium and yttrium complexes of a three-electron reduction product in the activation of dinitrogen, the $(N_2)^{3-}$ radical. J Am Chem Soc 131:11195–11202. doi:10.1021/ja9036753
21. Gelerinter E, Silsbee RH (1966) Electron spin resonance identification of an N_2^- defect in X-irradiated sodium azide. J Chem Phys 45:1703–1709. doi:10.1063/1.1727818
22. Marinkas PL, Bartram RH (1968) ESR of N_2^- in UV-irradiated single crystals of anhydrous barium azide. J Chem Phys 48:927–930. doi:10.1063/1.1668738
23. Brailsford JR, Morton JR, Vannotti LE (1969) Electron spin resonance spectrum of N_2^- trapped in KCl, KBr, and KI. J Chem Phys 50:1051–1055. doi:10.1063/1.1671155
24. Chiesa M, Giamello E, Murphy DM, Pacchioni G, Paganini MC, Soave R, Sojka Z (2001) Reductive activation of the nitrogen molecule at the surface of "electron-rich" MgO and CaO. The N_2^- surface adsorbed radical ion. J Phys Chem B 105:497–505. doi:10.1021/jp002794+
25. Bozkaya U, Turney JM, Yamaguchi Y, Schaefer III HF (2010) The barrier height, unimolecular rate constant, and lifetime for the dissociation of HN_2. J Chem Phys 132:064308. doi:10.1063/1.3310285
26. Stoicheff BP (1954) High resolution raman spectroscopy of gases: III. Raman spectrum of nitrogen. Can J Phys 32:630–634. doi:10.1139/p54-066
27. Carlotti M, Johns JWC, Trombetti A (1974) The ν_5 fundamental bands of N_2H_2 and N_2D_2. Can J Phys 52:340–344. doi:10.1139/p74-048
28. Craig NC, Levin IW (1979) Vibrational assignment and potential function for *trans*-diazene (diimide): predictions for *cis*-diazene. J Chem Phys 71:400. doi:10.1063/1.438084
29. Goubeau J, Kull U (1962) Die Schwingungsspektren von Natrium- und Zinkhydrazid. Z Anorg Allg Chem 316:182–189. doi:10.1002/zaac.19623160310
30. Shaver MP, Fryzuk MD (2003) Activation of molecular nitrogen: coordination, cleavage and functionalization of N_2 mediated by metal complexes. Adv Synth Catal 345:1061–1076. doi:10.1002/adsc.200303081
31. Studt F, Tuczek F (2006) Theoretical, spectroscopic, and mechanistic studies on transition-metal dinitrogen complexes: implications to reactivity and relevance to the nitrogenase problem. J Comput Chem 27:1278–1291. doi:10.1002/jcc.20413
32. Treitel IM, Flood MT, Marsh RE, Gray HB (1969) Molecular and electronic structure of μ-nitrogen-decaamminediruthenium(II). J Am Chem Soc 91:6512–6513. doi:10.1021/ja01051a070
33. Chatt J, Fay RC, Richards RL (1971) Preparation and characterisation of the dinuclear dinitrogen complex, trichloro-μ-dinitrogen-bis(tetrahydrofuran){chlorotetrakis[dimethyl-(phenyl)phosphine]rhenium(I)}chromium(III) $[(PMe_2Ph)_4ClReN_2CrCl_3\text{-}(thf)_2]$. J Chem Soc A 702–704. doi: 10.1039/J19710000702
34. Powell CB, Hall MB (1984) Molecular orbital calculations on dinitrogen-bridged transition-metal dimers. Inorg Chem 23:4619–4627. doi:10.1021/ic00194a042
35. Mercer M, Crabtree RH, Richards RL (1973) A μ-dinitrogen complex with a long N–N bond. X-ray crystal structure of $[(PMe_2Ph)_4ClReN_2MoCl_4(OMe)]$. J Chem Soc Chem Commun 808–809. doi: 10.1039/C39730000808

36. Laplaza CE, Johnson MJA, Peters JC, Odom AL, Kim E, Cummins CC, George GN, Pickering IJ (1996) Dinitrogen cleavage by three-coordinate molybdenum(III) complexes: mechanistic and structural data. J Am Chem Soc 118:8623–8638. doi:10.1021/ja960574x
37. Curley JJ, Cook TR, Reece SY, Müller P, Cummins CC (2008) Shining light on dinitrogen cleavage: structural features, redox chemistry, and photochemistry of the key intermediate bridging dinitrogen complex. J Am Chem Soc 130:9394–9405. doi:10.1021/ja8002638
38. Laplaza CE, Cummins CC (1995) Dinitrogen cleavage by a three-coordinate molybdenum (III) complex. Science 268:861–863. doi:10.1126/science.268.5212.861
39. Hirotsu M, Fontaine PP, Epshteyn A, Zavalij PY, Sita LR (2007) Dinitrogen activation at ambient temperatures: new modes of H_2 and $PhSiH_3$ additions for an "end-on-bridged" [Ta (IV)]$_2$(μ-η^1:η^1-N_2) complex and for the bis(μ-nitrido) [Ta(V)(μ-N)]$_2$ product derived from facile N≡N bond cleavage. J Am Chem Soc 129:9284–9285. doi:10.1021/ja072248v
40. Fontaine PP, Yonke BL, Zavalij PY, Sita LR (2010) Dinitrogen complexation and extent of N≡N activation within the group 6 "end-on-bridged" dinuclear complexes, {(η^5-C_5Me_5)M[N (i-Pr)C(Me)N(i-Pr)]}$_2$(μ-η^1:η^1-N_2) (M=Mo and W). J Am Chem Soc 132:12273–12285. doi:10.1021/ja100469f
41. Keane AJ, Yonke BL, Hirotsu M, Zavalij PY, Sita LR (2014) Fine-tuning the energy barrier for metal-mediated dinitrogen N≡N bond cleavage. J Am Chem Soc 136:9906–9909. doi:10.1021/ja505309j
42. Peigné B, Cano J, Aullón G (2012) On the coordination of dinitrogen to group 4 metallocenes. Eur J Inorg Chem 797–806. doi: 10.1002/ejic.201100788
43. Hirotsu M, Fontaine PP, Zavalij PY, Sita LR (2007) Extreme N≡N bond elongation and facile N-atom functionalization reactions within two structurally versatile new families of group 4 bimetallic "side-on-bridged" dinitrogen complexes for zirconium and hafnium. J Am Chem Soc 129:12690–12692. doi:10.1021/ja0752989
44. Bezdek MJ, Guo S, Chirik PJ (2016) Terpyridine molybdenum dinitrogen chemistry: synthesis of dinitrogen complexes that vary by five oxidation states. Inorg Chem 55:3117–3127. doi:10.1021/acs.inorgchem.6b00053
45. MacLachlan EA, Fryzuk MD (2006) Synthesis and reactivity of side-on-bound dinitrogen metal complexes. Organometallics 25:1530–1543. doi:10.1021/om051055i
46. Fryzuk MD, Haddad TS, Mylvaganam M, McConville DH, Rettig SJ (1993) End-on versus side-on bonding of dinitrogen to dinuclear early transition-metal complexes. J Am Chem Soc 115:2782–2792. doi:10.1021/ja00060a028
47. Armor JN, Taube H (1970) Linkage isomerization in nitrogen-labeled [Ru(NH_3)$_5$$N_2$]$Br_2$. J Am Chem Soc 92:2560–2562. doi:10.1021/ja00711a066
48. Jonas K (1973) π-Bonded nitrogen in a crystalline nickel-lithium complex. Angew Chem Int Ed Engl 12:997–998. doi:10.1002/anie.197309971
49. Krüger C, Tsay YH (1973) Molecular structure of a π-dinitrogen-nickel-lithium complex. Angew Chem Int Ed Engl 12:998–999. doi:10.1002/anie.197309981
50. Evans WJ, Ulibarri TA, Ziller JW (1988) Isolation and X-ray crystal structure of the first dinitrogen complex of an f-element metal, [(C_5Me_5)$_2$Sm]$_2$$N_2$. J Am Chem Soc 110:6877–6879. doi:10.1021/ja00228a043
51. Fryzuk MD, Haddad TS, Rettig SJ (1990) Reduction of dinitrogen by a zirconium phosphine complex to form a side-on-bridging N_2 ligand. Crystal structure of {[$Pr^i_2PCH_2SiMe_2$)$_2$N] ZrCl}$_2$(μ-η^2:η^2-N_2). J Am Chem Soc 112:8185–8186. doi: 10.1021/ja00178a063
52. Thorn DL, Tulip TH, Ibers JA (1979) The structure of *trans*-chloro(dinitrogen)bis(tri-isopropylphosphine)-rhodium(I): an *X*-ray study of the structure in the solid state and a nuclear magnetic resonance study of the structure in solution. J Chem Soc Dalton Trans 2022–2025. doi: 10.1039/dt9790002022
53. Peterson EJ, Von Dreele RB, Brown TM (1976) Crystal and molecular structure of tetraisothiocyanatobis(2,2′-bipyridine)niobium(IV) and -zirconium(IV). Inorg Chem 15:309–315. doi:10.1021/ic50156a014

54. Archer RD, Day RO, Illingsworth ML (1979) Transition-metal eight-coordination. 13. Synthesis, characterization, and crystal and molecular structure of the Schiff-base chelate bis(*N*,*N*′-disalicylidene-1,2-phenylenediamino)zirconium(IV) benzene solvate. Inorg Chem 18:2908–2916. doi:10.1021/ic50200a056
55. Studt F, Morello L, Lehnert N, Fryzuk MD, Tuczek F (2003) Side-on bridging coordination of N_2: spectroscopic characterization of the planar Zr_2N_2 core and theoretical investigation of its butterfly distortion. Chem A Eur J 9:520–530. doi:10.1002/chem.200390055
56. Clentsmith GKB, Bates VME, Hitchcock PB, Cloke FGN (1999) Reductive cleavage of dinitrogen by a vanadium diamidoamine complex: the molecular structures of [V($Me_3SiN\{CH_2CH_2NSiMe_3\}_2$)(μ-N)]$_2$ and K[V($Me_3SiN\{CH_2CH_2NSiMe_3\}_2$)(μ-N)]$_2$. J Am Chem Soc 121:10444–10445. doi:10.1021/ja9921219
57. Bates VME, Clentsmith GKB, Cloke GN, Green JC, Jenkin HDL (2000) Theoretical investigation of the pathway for reductive cleavage of dinitrogen by a vanadium diamidoamine complex. Chem Commun 927–928. doi: 10.1039/b002534h
58. Studt F, Lamarche VME, Clentsmith GKB, Cloke FGN, Tuczek F (2005) Vibrational and electronic structure of the dinuclear bis(μ-nitrido) vanadium(V) complex [V($N\{N''\}_2$)(μ-N)]$_2$: spectroscopic properties of the $M_2(\mu\text{-}N)_2$ diamond core. Dalton Trans 1052–1057. doi: 10.1039/b418856j
59. Zhang W, Tang Y, Lei M, Morokuma K, Musaev DG (2011) Ditantalum dinitrogen complex: reaction of H_2 molecule with "end-on-bridged" [Ta^{IV}]$_2$(μ-η^1:η^1-N_2) and bis(μ-nitrido) [Ta^{V}]$_2$(μ-N)$_2$ complexes. Inorg Chem 50:9481–9490. doi:10.1021/ic201159z
60. Cavigliasso G, Wilson L, McAlpine S, Attar M, Stranger R, Yates BF (2010) Activation and cleavage of the N–N bond in side-on bound [$L_2M\text{-}NN\text{-}ML_2$] (L=$NH_2$, NMe_2, N^iPr_2, C_5H_5, C_5Me_4H) dinitrogen complexes of transition metals from groups 4 through 9. Dalton Trans 39:4529–4540. doi:10.1039/b924999k
61. Bobadova-Parvanova P, Wang Q, Morokuma K, Musaev DG (2005) How many methyl groups in [{(η^5-$C_5Me_nH_{5-n}$)$_2$Zr}$_2$(μ_2,η^2,η^2-N_2)] are needed for dinitrogen hydrogenation? A theoretical study. Angew Chem Int Ed 44:7101–7103. doi:10.1002/anie.200501371
62. Chirik PJ (2010) Group 4 transition metal sandwich complexes: still fresh after almost 60 years. Organometallics 29:1500–1517. doi:10.1021/om100016p
63. Pool JA, Lobkovsky E, Chirik PJ (2004) Hydrogenation and cleavage of dinitrogen to ammonia with a zirconium complex. Nature 427:527–530. doi:10.1038/nature02274
64. Manriquez JM, Bercaw JE (1974) Preparation of a dinitrogen complex of bis(pentamethylcyclopentadienyl)zirconium(II). Isolation and protonation leading to stoichiometric reduction of dinitrogen to hydrazine. J Am Chem Soc 96:6229–6230. doi:10.1021/ja00826a071
65. Pool JA, Bernskoetter WH, Chirik PJ (2004) On the origin of dinitrogen hydrogenation promoted by [(η^5-C_5Me_4H)$_2$Zr]$_2$(μ_2,η^2,η^2-N_2). J Am Chem Soc 126:14326–14327. doi:10.1021/ja045566s
66. Knobloch DJ, Lobkovsky E, Chirik PJ (2010) Dinitrogen cleavage and functionalization by carbon monoxide promoted by a hafnium complex. Nat Chem 2:30–35. doi:10.1038/nchem.477
67. Bobadova-Parvanova P, Wang Q, Quinonero-Santiago D, Morokuma K, Musaev DG (2006) Does dinitrogen hydrogenation follow different mechanisms for [(η^5-C_5Me_4H)$_2$Zr]$_2$(μ_2,η^2,η^2-N_2) and {[PhP($CH_2SiMe_2NSiMe_2CH_2$)PPh]Zr}$_2$(μ_2,η^2,η^2-N_2) complexes? A computational study. J Am Chem Soc 128:11391–11403. doi:10.1021/ja057937q
68. Fryzuk MD, Johnson SA, Rettig SJ (1998) New mode of coordination for the dinitrogen ligand: a dinuclear tantalum complex with a bridging N_2 unit that is both side-on and end-on. J Am Chem Soc 120:11024–11025. doi:10.1021/ja982377z
69. Fryzuk MD, Johnson SA, Patrick BO, Albinati A, Mason SA, Koetzle TF (2001) New mode of coordination for the dinitrogen ligand: formation, bonding, and reactivity of a tantalum complex with a bridging N_2 unit that is both side-on and end-on. J Am Chem Soc 123:3960–3973. doi:10.1021/ja0041371

70. Fryzuk MD, MacKay BA, Johnson SA, Patrick BO (2002) Hydroboration of coordinated dinitrogen: a new reaction for the N_2 ligand that results in its functionalization and cleavage. Angew Chem Int Ed 41:3709–3712. doi:10.1002/1521-3773(20021004)41:19<3709::aid-anie3709>3.0.co;2-u
71. Fryzuk MD, MacKay BA, Patrick BO (2003) Hydrosilylation of a dinuclear tantalum dinitrogen complex: cleavage of N_2 and functionalization of both nitrogen atoms. J Am Chem Soc 125:3234–3235. doi:10.1021/ja034303f
72. MacKay BA, Munha RF, Fryzuk MD (2006) Substituent effects in the hydrosilylation of coordinated dinitrogen in a ditantalum complex: cleavage and functionalization of N_2. J Am Chem Soc 128:9472–9483. doi:10.1021/ja061508q
73. Yeo A, Shaver MP, Fryzuk MD (2015) A new side-on end-on ditantalum dinitrogen complex and its reaction with $BuSiH_3$. Z Anorg Allg Chem 641:123–127. doi:10.1002/zaac.201400167
74. MacKay BA, Patrick BO, Fryzuk MD (2005) Hydroalumination of a dinuclear tantalum dinitrogen complex: N–N bond cleavage and ancillary ligand rearrangement. Organometallics 24:3836–3841. doi:10.1021/om050208z
75. Spencer LP, MacKay BA, Patrick BO, Fryzuk MD (2006) Inner-sphere two-electron reduction leads to cleavage and functionalization of coordinated dinitrogen. Proc Natl Acad Sci U S A 103:17094–17098. doi:10.1073/pnas.0602132103
76. Ballmann J, Yeo A, Patrick BO, Fryzuk MD (2011) Carbon-nitrogen bond formation by the reaction of 1,2-cumulenes with a ditantalum complex containing side-on- and end-on-bound dinitrogen. Angew Chem Int Ed 50:507–510. doi:10.1002/anie.201005704
77. Cui Q, Musaev DG, Svensson M, Sieber S, Morokuma K (1995) N_2 cleavage by three-coordinate group 6 complexes. W(III) Complexes would be better than Mo(III) complexes. J Am Chem Soc 117:12366–12367. doi:10.1021/ja00154a052
78. Peters JC, Cherry JPF, Thomas JC, Baraldo L, Mindiola DJ, Davis WM, Cummins CC (1999) Redox-catalyzed binding of dinitrogen by molybdenum *N-tert*-hydrocarbylanilide complexes: implications for dinitrogen functionalization and reductive cleavage. J Am Chem Soc 121:10053–10067. doi:10.1021/ja991435t
79. Kol M, Schrock RR, Kempe R, Davis WM (1994) Synthesis of molybdenum and tungsten complexes that contain triamidoamine ligands of the type $(C_6F_5NCH_2CH_2)_3N$ and activation of dinitrogen by molybdenum. J Am Chem Soc 116:4382–4390. doi:10.1021/ja00089a028
80. Shih KY, Schrock RR, Kempe R (1994) Synthesis of molybdenum complexes that contain silylated triamidoamine ligands. A μ-dinitrogen complex, methyl and acetylide complexes, and coupling of acetylides. J Am Chem Soc 116:8804–8805. doi:10.1021/ja00098a048
81. Christian G, Driver J, Stranger R (2003) Dinitrogen activation in sterically-hindered three-coordinate transition metal complexes. Faraday Discuss 124:331–341. doi:10.1039/b211335j
82. Christian G, Stranger R, Yates BF, Graham DC (2005) Ligand rotation in $[Ar(R)N]_3M\text{-}N_2\text{-}M'[N(R)Ar]_3$ ($M,M' = Mo^{III}$, Nb^{III}; R = ^{i}Pr and ^{t}Bu) dimers. Dalton Trans 962–968. doi: 10.1039/b413766c
83. Brookes NJ, Graham DC, Christian G, Stranger R, Yates BF (2009) The influence of peripheral ligand bulk on nitrogen activation by three-coordinate molybdenum complexes – a theoretical study using the ONIOM method. J Comput Chem 30:2146–2156. doi:10.1002/jcc.21199
84. Solari E, Da Silva C, Iacono B, Hesschenbrouck J, Rizzoli C, Scopelliti R, Floriani C (2001) Photochemical activation of the N≡N bond in a dimolybdenum–dinitrogen complex: formation of a molybdenum nitride. Angew Chem Int Ed 40:3907–3909. doi:10.1002/1521-3773(20011015)40:20<3907::aid-anie3907>3.0.co;2-#
85. Huss AS, Curley JJ, Cummins CC, Blank DA (2013) Relaxation and dissociation following photoexcitation of the $(\mu\text{-}N_2)[Mo(N[t\text{-}Bu]Ar)_3]_2$ dinitrogen cleavage intermediate. J Phys Chem B 117:1429–1436. doi:10.1021/jp310122x
86. Reiher M, Kirchner B, Hutter J, Sellmann D, Hess BA (2004) A photochemical activation scheme of inert dinitrogen by dinuclear Ru^{II} and Fe^{II} complexes. Chem A Eur J 10:4443–4453. doi:10.1002/chem.200400081

87. Chisholm MH, Cotton FA, Frenz BA, Reichert WW, Shive LW, Stults BR (1976) The molybdenum–molybdenum triple bond. 1. Hexakis(dimethy1amido)dimolybdenum and some homologues: preparation, structure, and properties. J Am Chem Soc 98:4469–4476. doi:10.1021/ja00431a024
88. Hahn J, Landis CR, Nasluzov VA, Neyman KM, Rösch N (1997) Steric effects on dinitrogen cleavage by three-coordinate molybdenum(III) complexes: a molecular mechanics study. Inorg Chem 36:3947–3951. doi:10.1021/ic961466e
89. Johnson MJA, Lee PM, Odom AL, Davis WM, Cummins CC (1997) Atom-bridged intermediates in N- and P-atom transfer reactions. Angew Chem Int Ed Engl 36:87–91. doi:10.1002/anie.199700871
90. Cummins CC (1998) Reductive cleavage and related reactions leading to molybdenum–element multiple bonds: new pathways offered by three-coordinate molybdenum(III). Chem Commun 1777–1786. doi: 10.1039/a802402b
91. Laplaza CE, Johnson AR, Cummins CC, October RV (1996) Nitrogen atom transfer coupled with dinitrogen cleavage and Mo–Mo triple bond formation. J Am Chem Soc 118:709–710. doi:10.1021/ja953573y
92. Tsai YC, Johnson MJA, Mindiola DJ, Cummins CC, Klooster WT, Koetzle TF (1999) A cyclometalated resting state for a reactive molybdenum amide: favorable consequences of β-hydrogen elimination including reductive cleavage, coupling, and complexation. J Am Chem Soc 121:10426–10427. doi:10.1021/ja9917464
93. van Koten G, Milstein D (eds) (2013) Organometallic pincer chemistry. Topics in organometallic chemistry, vol 40. Springer, Heidelberg
94. Szabo KJ, Wendt OF (eds) (2014) Pincer and pincer-type complexes: applications in organic synthesis and catalysis. Wiley-VCH, Weinheim
95. Smythe NC, Schrock RR, Müller P, Weare WW (2006) Synthesis of [(HIPTNCH$_2$CH$_2$)$_3$N]Cr compounds (HIPT=3,5-(2,4,6-*i*-Pr$_3$C$_6$H$_2$)$_2$C$_6$H$_3$) and an evaluation of chromium for the reduction of dinitrogen to ammonia. Inorg Chem 45:7111–7118. doi:10.1021/ic060549k
96. Vidyaratne I, Scott J, Gambarotta S, Budzelaar PHM (2007) Dinitrogen activation, partial reduction, and formation of coordinated imide promoted by a chromium diiminepyridine complex. Inorg Chem 46:7040–7049. doi:10.1021/ic700810f
97. Hebden TJ, Schrock RR, Takase MK, Müller P (2012) Cleavage of dinitrogen to yield a (*t*-BuPOCOP)molybdenum(IV) nitride. Chem Commun 48:1851–1853. doi:10.1039/c2cc17634c
98. Liao Q, Cavaillé A, Saffon-Merceron N, Mézailles N (2016) Direct synthesis of silylamine from N_2 and a silane: mediated by a tridentate phosphine molybdenum fragment. Angew Chem Int Ed 55:11212–11216. doi:10.1002/anie.201604812
99. Liao Q, Saffon-Merceron N, Mézailles N (2015) N_2 reduction into silylamine at tridentate phosphine/Mo center: catalysis and mechanistic study. ACS Catal 5:6902–6906. doi:10.1021/acscatal.5b01626
100. Arashiba K, Kinoshita E, Kuriyama S, Eizawa A, Nakajima K, Tanaka H, Yoshizawa K, Nishibayashi Y (2015) Catalytic reduction of dinitrogen to ammonia by use of molybdenum–nitride complexes bearing a tridentate triphosphine as catalysts. J Am Chem Soc 137:5666–5669. doi:10.1021/jacs.5b02579
101. Klopsch I, Finger M, Würtele C, Milde B, Werz DB, Schneider S (2014) Dinitrogen splitting and functionalization in the coordination sphere of rhenium. J Am Chem Soc 136:6881–6883. doi:10.1021/ja502759d
102. Klopsch I, Kinauer M, Finger M, Würtele C, Schneider S (2016) Conversion of dinitrogen into acetonitrile under ambient conditions. Angew Chem Int Ed 55:4786–4789. doi:10.1002/anie.201600790
103. Scheibel MG, Askevold B, Heinemann FW, Reijerse EJ, de Bruin B, Schneider S (2012) Closed-shell and open-shell square-planar iridium nitrido complexes. Nat Chem 4:552–558. doi:10.1038/nchem.1368

104. Scheibel MG, Wu Y, Stückl AC, Krause L, Carl E, Stalke D, de Bruin B, Schneider S (2013) Synthesis and reactivity of a transient, terminal nitrido complex of rhodium. J Am Chem Soc 135:17719–17722. doi:10.1021/ja409764j
105. Abbenseth J, Finger M, Würtele C, Kasanmascheff M, Schneider S (2016) Coupling of terminal iridium nitrido complexes. Inorg Chem Front 3:469–477. doi:10.1039/c5qi00267b
106. Keane AJ, Farrell WS, Yonke BL, Zavalij PY, Sita LR (2015) Metal-mediated production of isocyanates, $R_3EN{=}C{=}O$ from dinitrogen, carbon dioxide, and R_3ECl. Angew Chem Int Ed 54:10220–10224. doi:10.1002/anie.201502293
107. Miyazaki T, Tanaka H, Tanabe Y, Yuki M, Nakajima K, Yoshizawa K, Nishibayashi Y (2014) Cleavage and formation of molecular dinitrogen in a single system assisted by molybdenum complexes bearing ferrocenyldiphosphine. Angew Chem Int Ed 53:11488–11492. doi:10.1002/anie.201405673
108. Rebreyend C, de Bruin B (2015) Photolytic N_2 splitting: a road to sustainable NH_3 production? Angew Chem Int Ed 54:42–44. doi:10.1002/anie.201409727
109. Crossland JL, Tyler DR (2010) Iron–dinitrogen coordination chemistry: dinitrogen activation and reactivity. Coord Chem Rev 254:1883–1894. doi:10.1016/j.ccr.2010.01.005
110. Khoenkhoen N, de Bruin B, Reek JNH, Dzik WI (2015) Reactivity of dinitrogen bound to mid- and late-transition-metal centers. Eur J Inorg Chem 567–598. doi: 10.1002/ejic.201403041
111. McWilliams SF, Holland PL (2015) Dinitrogen binding and cleavage by multinuclear iron complexes. Acc Chem Res 48:2059–2065. doi:10.1021/acs.accounts.5b00213
112. Hazari N (2010) Homogeneous iron complexes for the conversion of dinitrogen into ammonia and hydrazine. Chem Soc Rev 39:4044–4056. doi:10.1039/b919680n
113. MacLeod KC, Holland PL (2013) Recent developments in the homogeneous reduction of dinitrogen by molybdenum and iron. Nat Chem 5:559–565. doi:10.1038/nchem.1620
114. Betley TA, Peters JC (2004) A tetrahedrally coordinated $L_3Fe{-}N_x$ platform that accommodates terminal nitride ($Fe^{IV}{\equiv}N$) and dinitrogen ($Fe^{I}{-}N_2{-}Fe^{I}$) ligands. J Am Chem Soc 126:6252–6254. doi:10.1021/ja048713v
115. Hendrich MP, Gunderson W, Behan RK, Green MT, Mehn MP, Betley TA, Lu CC, Peters JC (2006) On the feasibility of N_2 fixation via a single-site Fe^{I}/Fe^{IV} cycle: spectroscopic studies of $Fe^{I}(N_2)Fe^{I}$, $Fe^{IV}{\equiv}N$, and related spiecies. Proc Natl Acad Sci U S A 103:17107–17112. doi:10.1073/pnas.0604402103
116. Krahe O, Bill E, Neese F (2014) Decay of iron(V) nitride complexes by a N–N bond-coupling reaction in solution: a combined spectroscopic and theoretical analysis. Angew Chem Int Ed 53:8727–8731. doi:10.1002/anie.201403402
117. Kane-Maguire LAP, Sheridan PS, Basolo F, Pearson RG (1970) Azidoruthenium(III) complexes as precursors for molecular nitrogen and nitrene complexes. J Am Chem Soc 92:5865–5872. doi:10.1021/ja00723a009
118. Buhr JD, Taube H (1979) Oxidation of $[Os(NH_3)_5CO]^{2+}$ to $[(Os(NH_3)_4CO)_2N_2]^{4+}$. Inorg Chem 18:2208–2212. doi:10.1021/ic50198a032
119. Che CM, Lam HW, Tong WF, Lai TF, Lau TC (1989) Model reactions for nitrogen fixation. Photo-induced formation and X-ray crystal structure of $[Os_2(NH_3)_8(MeCN)_2(N_2)]^{5+}$ from $[Os^{VI}(NH_3)_4N]^{3+}$. J Chem Soc Chem Commun 1883–1884. doi: 10.1039/c39890001883
120. Ware DC, Taube H (1991) Substitution-induced N–N coupling for nitride coordinated to osmium(VI). Inorg Chem 30:4605–4610. doi:10.1021/ic00024a029
121. Demadis KD, Meyer TJ, White PS (1997) Localization in *trans*,*trans*-$[(tpy)(Cl)_2Os^{III}(N_2)Os^{II}(Cl)_2(tpy)]^{+}$ (tpy=2,2′:6′,2″-Terpyridine). Inorg Chem 36:5678–5679. doi:10.1021/ic970885o
122. Seymore SB, Brown SN (2002) Polar effects in nitride coupling reactions. Inorg Chem 41:462–469. doi:10.1021/ic010844z
123. Kunkely H, Vogler A (2010) Photolysis of aqueous $[(NH_3)_5Os(\mu\text{-}N_2)Os(NH_3)_5]^{5+}$: cleavage of dinitrogen by an intramolecular photoredox reaction. Angew Chem Int Ed 49:1591–1593. doi:10.1002/anie.200905026
124. Rodriguez MM, Bill E, Brennessel WW, Holland PL (2011) N_2 reduction and hydrogenation to ammonia by a molecular iron-potassium complex. Science 334:780–783. doi:10.1126/science.1211906

125. Smith JM, Lachicotte RJ, Pittard KA, Cundari TR, Lukat-Rodgers G, Rodgers KR, Holland PL (2001) Stepwise reduction of dinitrogen bond order by a low-coordinate iron complex. J Am Chem Soc 123:9222–9223. doi:10.1021/ja016094+
126. Figg TM, Holland PL, Cundari TR (2012) Cooperativity between low-valent iron and potassium promoters in dinitrogen fixation. Inorg Chem 51:7546–7550. doi:10.1021/ic300150u
127. Grubel K, Brennessel WW, Mercado BQ, Holland PL (2014) Alkali metal control over N−N cleavage in iron complexes. J Am Chem Soc 136:16807–16816. doi:10.1021/ja507442b
128. McWilliams SF, Rodgers KR, Lukat-Rodgers G, Mercado BQ, Grubel K, Holland PL (2016) Alkali metal variation and twisting of the FeNNFe core in bridging diiron dinitrogen complexes. Inorg Chem 55:2960–2968. doi:10.1021/acs.inorgchem.5b02841
129. MacLeod KC, Vinyard DJ, Holland PL (2014) A multi-iron system capable of rapid N_2 formation and N_2 cleavage. J Am Chem Soc 136:10226–10229. doi:10.1021/ja505193z
130. MacLeod KC, McWilliams SF, Mercado BQ, Holland PL (2016) Stepwise N–H bond formation from N_2-derived iron nitride, imide and amide intermediates to ammonia. Chem Sci 7:5736–5746. doi:10.1039/c6sc00423g
131. MacLeod KC, Menges FS, McWilliams SF, Craig SM, Mercado BQ, Johnson MA, Holland PL (2016) Alkali-controlled C–H cleavage or N–C bond formation by N_2-derived iron nitrides and imides. J Am Chem Soc 138:11185–11191. doi:10.1021/jacs.6b04984
132. Lee Y, Sloane FT, Blondin G, Abboud KA, García-Serres R, Murray LJ (2015) Dinitrogen activation upon reduction of a triiron(II) complex. Angew Chem Int Ed 54:1499–1503. doi:10.1002/anie.201409676
133. Eikey RA, Abu-Omar MM (2003) Nitrido and imido transition metal complexes of groups 6–8. Coord Chem Rev 243:83–124. doi:10.1016/S0010-8545(03)00048-1
134. Berry JF (2009) Terminal nitrido and imido complexes of the late transition metals. Comm Inorg Chem 30:28–66. doi:10.1080/02603590902768875
135. Shima T, Hu S, Luo G, Kang X, Luo Y, Hou Z (2013) Dinitrogen cleavage and hydrogenation by a trinuclear titanium polyhydride complex. Science 340:1549–1552. doi:10.1126/science.1238663
136. Nikiforov GB, Vidyaratne I, Gambarotta S, Korobkov I (2009) Titanium-promoted dinitrogen cleavage, partial hydrogenation, and silylation. Angew Chem Int Ed 48:7415–7419. doi:10.1002/anie.200903648
137. Vidyaratne I, Crewdson P, Lefebvre E, Gambarotta S (2007) Dinitrogen coordination and cleavage promoted by a vanadium complex of a σ,π,σ-donor ligand. Inorg Chem 46:8836–8842
138. Akagi F, Matsuo T, Kawaguchi H (2007) Dinitrogen cleavage by a diniobium tetrahydride complex: formation of a nitride and its conversion into imide species. Angew Chem Int Ed 46:8778–8781. doi:10.1002/anie.200703336
139. Searles K, Carroll PJ, Chen CH, Pink M, Mindiola DJ (2015) Niobium-nitrides derived from nitrogen splitting. Chem Commun 51:3526–3528. doi:10.1039/c4cc09563d
140. Andino JG, Mazumder S, Pal K, Caulton KG (2013) New approaches to functionalizing metal-coordinated N_2. Angew Chem Int Ed 52:4726–4732. doi:10.1002/anie.201209168
141. Benson SW (1965) Bond energies. J Chem Educ 42:502–518. doi:10.1021/ed042p502
142. Burgess DR. Thermochemical data. In: Linstrom PJ, Mallard WG (eds) NIST chemistry WebBook, NIST standard reference database number 69. National Institute of Standards and Technology, Gaithersburg MD. http://webbook.nist.gov
143. Kawaguchi H, Matsuo T (2002) Dinitrogen-bond cleavage in a niobium complex supported by a tridentate aryloxide ligand. Angew Chem Int Ed 41:2792–2794. doi:10.1002/1521-3773(20020802)41:15<2792::aid-anie2792>3.0.co;2-k
144. Akagi F, Suzuki S, Ishida Y, Hatanaka T, Matsuo T, Kawaguchi H (2013) Reactions of a niobium nitride complex prepared from dinitrogen: synthesis of imide and ureate complexes and ammonia formation. Eur J Inorg Chem 3930–3936. doi: 10.1002/ejic.201300172
145. Ishida Y, Kawaguchi H (2014) Nitrogen atom transfer from a dinitrogen-derived vanadium nitride complex to carbon monoxide and isocyanide. J Am Chem Soc 136:16990–16993. doi:10.1021/ja510317h

146. Yonke BL, Reeds JP, Fontaine PP, Zavalij PY, Sita LR (2014) Catalytic production of isocyanates via orthogonal atom and group transfers employing a shared formal group 6 M (II)/M(IV) redox cycle. Organometallics 33:3239–3242. doi:10.1021/om500532s
147. Cozzolino AF, Silvia JS, Lopez N, Cummins CC (2014) Experimental and computational studies on the formation of cyanate from early metal terminal nitrido ligands and carbon monoxide. Dalton Trans 43:4639–4652. doi:10.1039/c3dt52738g
148. Silvia JS, Cummins CC (2009) Two-electron reduction of a vanadium(V) nitride by CO to release cyanate and open a coordination site. J Am Chem Soc 131:446–447. doi:10.1021/ja807767w
149. Tran BL, Pink M, Gao X, Park H, Mindiola DJ (2010) Low-coordinate and neutral nitrido complexes of vanadium. J Am Chem Soc 132:1458–1459. doi:10.1021/ja908303k
150. Sceats EL, Figueroa JS, Cummins CC, Loening NM, Van der Wel P, Griffin RG (2004) Complexes obtained by electrophilic attack on a dinitrogen-derived terminal molybdenum nitride: electronic structure analysis by solid state CP/MAS ^{15}N NMR in combination with DFT calculations. Polyhedron 23:2751–2768. doi:10.1016/j.poly.2004.08.010
151. Curley JJ, Cozzolino AF, Cummins CC (2011) Nitrogen fixation to cyanide at a molybdenum center. Dalton Trans 40:2429–2432. doi:10.1039/c0dt01326a
152. Sivasankar C, Tuczek F (2006) Double deprotonation of coordinated ethylimide to CH_3CN: molecular mechanism and relevance to the chemistry of Mo and W organoimides. Dalton Trans 3396–3398. doi: 10.1039/b602038k
153. Kukushkin VY, Pombeiro AJL (2002) Additions to metal-activated organonitriles. Chem Rev 102:1771–1802. doi:10.1021/cr0103266
154. Henderickx H, Kwakkenbos G, Peters A, van der Spoel J, de Vries K (2003) Direct formation of an organonitrogen compound from a molybdenum nitrido species. Chem Commun 897:2050–2051. doi:10.1039/b305774g
155. Curley JJ, Sceats EL, Cummins CC (2006) A cycle for organic nitrile synthesis via dinitrogen cleavage. J Am Chem Soc 128:14036–14037. doi:10.1021/ja066090a
156. Mindiola DJ, Meyer K, Cherry JPF, Baker TA, Cummins CC (2000) Dinitrogen cleavage stemming from a heterodinuclear niobium/molybdenum N_2 complex: new nitridoniobium systems including a niobazene cyclic trimer. Organometallics 19:1622–1624. doi:10.1021/om000159k
157. Figueroa JS, Piro NA, Clough CR, Cummins CC (2006) A nitridoniobium(V) reagent that effects acid chloride to organic nitrile conversion: synthesis via heterodinuclear (Nb/Mo) dinitrogen cleavage, mechanistic insights, and recycling. J Am Chem Soc 128:940–950. doi:10.1021/ja056408j
158. Hou Z, Shima T, Hu S, Endo Y (2014) Novel complex and use of same. WO Patent 2014080939 A1, US Patent 20150291635
159. Hu S, Shima T, Luo Y, Hou Z (2013) Tetranuclear zirconium and hafnium polyhydride complexes composed of the "$CpMH_2$" units. Organometallics 32:2145–2151. doi:10.1021/om400012a
160. Guru MM, Shima T, Hou Z (2016) Conversion of dinitrogen to nitriles at a multinuclear titanium framework. Angew Chem Int Ed. doi: 10.1002/anie.201607426
161. Askevold B, Nieto JT, Tussupbayev S, Diefenbach M, Herdweck E, Holthausen MC, Schneider S (2011) Ammonia formation by metal-ligand cooperative hydrogenolysis of a nitrido ligand. Nat Chem 3:532–537. doi:10.1038/nchem.1051
162. Schendzielorz FS, Finger M, Volkmann C, Würtele C, Schneider S (2016) A terminal osmium(IV) nitride: ammonia formation and ambiphilic reactivity. Angew Chem Int Ed 55:11417–11420. doi:10.1002/anie.201604917
163. Walstrom A, Fan H, Pink M, Caulton KG (2010) Unexpected selectivity in electrophilic attack on (PNP)RuN. Inorg Chim Acta 363:633–636. doi:10.1016/j.ica.2008.11.010